



# The leading interannual variability modes of winter surface air temperature over Southeast Asia

Shangfeng Chen<sup>1</sup> · Linye Song<sup>2</sup>

Received: 31 December 2017 / Accepted: 13 August 2018 / Published online: 16 August 2018  
© Springer-Verlag GmbH Germany, part of Springer Nature 2018

## Abstract

The present study analyzes the leading interannual variability modes of Southeast Asian surface air temperature (SAT) during boreal winter. The first Empirical Orthogonal Function (EOF1) mode displays same-sign SAT anomalies over Southeast Asia, with a center around the north Indo-China Peninsula and south China. The second EOF (EOF2) shows a dipole SAT anomaly pattern between the Indo-China Peninsula and south China. Surface heat flux change may not be able to explain SAT variation related to the EOF1, but explain partly the SAT change associated with the EOF2. Atmospheric anomalies play a crucial role in the SAT variations via wind-induced temperature advection. Specifically, for the EOF1, marked northerly anomalies appear over the Southeast Asia, which bring colder air from higher latitude and contribute to negative SAT anomalies. Change in the intensity of Arctic Oscillation, Siberian High and La Niña like sea surface temperature (SST) anomalies over the tropical central-eastern Pacific play a key role in forming the northerly anomalies related to the EOF1. For the EOF2, at the lower troposphere, a pair of anomalous cyclones appears over the tropical north and south Indian Ocean, together with southwesterly wind anomalies extending from the Indian Ocean to the Indo-China Peninsula, which favor positive SAT anomalies there. Formation of the twin cyclones is likely to be a Gill type Rossby wave response of the tropical Indian Ocean SST warming. At the upper troposphere, two wave trains, one originated from the Arctic region and another from the Mediterranean Sea, contribute collectively to the atmospheric circulation anomalies over Southeast Asia related to the EOF2.

**Keywords** Southeast Asia · Surface air temperature · Atmospheric circulation · Sea surface temperature

## 1 Introduction

Changes in the surface air temperature (SAT) can exert substantial influences on the natural systems, socioeconomic development, and people's daily activity (e.g., Kunkel et al. 1999; Keellings and Waylen 2012; IPCC 2013; Guan et al. 2015; Caloiero 2017). Many environmental aspects were impacted by SAT changes, including crop growth, food

safety assessment, and agro-ecological zoning (Yao 1995; Ye et al. 2013). The extremely high SAT in summer of 2003 resulted in broad wildfires and large economic loss over many European countries (e.g., Beniston 2004; Stott et al. 2004; Feudale and Shukla 2010). The abnormally hot temperature in eastern China in July and August of 2013 exerts notable impacts on the local agricultural yields and people's daily lives (e.g., Sun et al. 2014; Xia et al. 2016). In addition, the freezing rain and the associated extremely low SAT in the early of 2008 bring huge damage to the agriculture, electricity, and transportation systems over south China (e.g., Bao et al. 2010; Zuo et al. 2016a). Studies found that SAT variations are able to influence the evapotranspiration rates and soil moisture, which further lead to change in the water and energy exchange between the lower atmosphere and surface land (e.g., Henderson-Sellers 1996; Labat et al. 2004). Eurasian SAT variations also influence the temperature differences between the surrounding oceans and the continent, which further lead to change in the Asian monsoon activity

**Electronic supplementary material** The online version of this article (<https://doi.org/10.1007/s00382-018-4406-x>) contains supplementary material, which is available to authorized users.

✉ Shangfeng Chen  
chenshangfeng@mail.iap.ac.cn

<sup>1</sup> Center for Monsoon System Research, Institute of Atmospheric Physics, Chinese Academy of Sciences, Beijing 100029, China

<sup>2</sup> Institute of Urban Meteorology, China Meteorological Administration, Beijing, China

(Liu and Yanai 2001; D'Arrigo et al. 2006). Thereby, it is crucial to investigate the SAT variability.

Several studies have examined the dominant modes of the SAT variations over different regions of Eurasia (e.g., Miyazaki and Yasunari 2008; Zveryaev and Gulev 2009; Chen et al. 2016a, b). Miyazaki and Yasunari (2008) showed that the first Empirical orthogonal Function (EOF) mode of winter SAT variation over Asia and the surrounding oceans displays a north–south dipole anomaly pattern between high latitude of Asia and the tropical Ocean, which is closely connected with the Arctic Oscillation (AO) and cold surge variability. The second EOF mode displays an inner-Asian mode with a center of action to the north of the Tibetan Plateau. The second EOF mode is related to the Siberian High and the Icelandic Low. Chen et al. (2016b) found that the first EOF mode of summertime northeast Asian SAT interannual variation is featured by same-sign SAT change and it is related to an eastward propagating atmospheric wave train over the Eurasia. The second EOF mode displays a north–south dipole anomaly pattern, which is associated with the East Asian Pacific teleconnection pattern (also called Pacific–Japan teleconnection pattern) (Nitta 1987; Huang and Sun 1992). Furthermore, Chen et al. (2016a) have investigated the leading interannual variability modes of the spring SAT over the mid-high latitudes of Eurasia. Their results show that spring AO-related atmospheric circulation changes play a key role for the formation of the SAT anomalies related to the first EOF mode mainly via wind-induced temperature advection. SAT anomalies related to the second EOF mode were closely associated with an anomalous atmospheric wave train over North Atlantic through Eurasia, which may be triggered by the North Atlantic tripole sea surface temperature (SST) anomaly pattern.

Several studies have investigated the SAT variability over Southeast Asian region, but mainly focus on the long-term change and on sub-regions of Southeast Asia (e.g., Nguyen et al. 2014; Cinco et al. 2014; Chooprteep and McNeil 2016). For instance, Nguyen et al. (2014) showed that the surface temperature averaged in Vietnam has increased at a rate of  $0.26 \pm 0.10$  °C per decade during 1971–2010. The increasing rate is larger in winter than in summer (Nguyen et al. 2014). Chooprteep and McNeil (2016) have examined the SAT long-term change from 1909 to 2008 over Southeast Asia via the factor analysis method. They showed that SAT was increasing in most of the Southeast Asian region during 1909–1944 with a rate ranging from 0.005 to 0.148 °C per decade. While during 1973–2008, the increasing rate ranges from 0.082 to 0.222 °C per decade for the SAT change.

At present, it is still unclear regarding the spatial structures of the dominant modes of boreal winter SAT variations on the interannual timescale over the Southeast Asian region. It is also unclear about the factors responsible for the SAT anomalies related to the dominant interannual

variability of the winter Southeast Asian SAT variations. It is noted that abnormal SAT variations over Southeast Asia can exert large impacts on regional socioeconomic development and people's daily lives. For example, the extremely cold SAT anomaly in February 2008 resulted in substantial fishery and agriculture losses in the Southeast Asian regions (Hong and Li 2009). In addition, the record-breaking warm SAT in April 2016 led to significant impacts on crop production, energy consumption and people's lives (Nirmal 2016; Thirumalai et al. 2017). Hence, it is important to improve our understanding about the SAT variability over the Southeast Asia and the related factors. The goal of the present study is to examine the leading patterns of winter Southeast Asian SAT anomalies on the interannual time scale. We also investigate the possible factors contributing to the Southeast Asian SAT changes related to the dominant modes. The rest of this paper is organized as follows: Sect. 2 describes the data and methods employed in this study. Section 3 analyzes the dominant modes of interannual variation of winter SAT over Southeast Asia. Section 4 investigates the factors responsible for Southeast Asian SAT interannual variations, including atmospheric circulation, SST, and Arctic sea ice changes. Section 5 provides a summary.

## 2 Data and methods

Monthly SST data employed in the present study were derived from the National Oceanic and Atmospheric Administration (NOAA) Extended Reconstructed SST, version 5 (ERSSTv5) dataset (Huang et al. 2017; Available online <https://www.esrl.noaa.gov/psd/data/gridded/data.noaa.ersst.v5.html>). We also used the SST data derived from the ERSSTv3b (Smith et al. 2008; <https://www.esrl.noaa.gov/psd/data/gridded/data.noaa.ersst.v3.html>) and from the Hadley Centre Sea Ice and Sea Surface Temperature dataset (HadISST; Rayner et al. 2003; <http://www.metoffice.gov.uk/hadobs/hadisst>). The SST data derived from the ERSSTv5 and ERSSTv3b both have a horizontal resolution of  $2^\circ \times 2^\circ$  and are available from 1854 to the present. The SST data derived from the HadISST has a horizontal resolution of  $1^\circ \times 1^\circ$  and are available from 1870 to the present. The results obtained in this paper are highly similar among the three SST datasets (i.e., ERSSTv5, ERSSTv3b and HadISST). Thus, we only show the results obtained from the ERSSTv5. It is noted that the results based on the ERSSTv3b and HadISST are shown in the supporting materials.

Monthly precipitation data were obtained from the Global Precipitation Climatology Project (GPCP) from 1979 to the present, which has a horizontal resolution of  $2.5^\circ \times 2.5^\circ$  (Adler et al. 2003; <http://www.esrl.noaa.gov/psd/data/gridded/data.gpcp.html>). We also use the monthly sea ice concentration (SIC) data from the Hadley Centre Sea Ice and Sea

Surface Temperature dataset (HadISST) since 1870 with a horizontal resolution of  $1^\circ \times 1^\circ$  (Rayner et al. 2003; <http://www.metoffice.gov.uk/hadobs/hadisst>). Monthly sea level pressure (SLP), winds at 1000 hPa, geopotential height, total cloud cover, and surface heat fluxes (including surface sensible and latent heat fluxes, surface longwave and shortwave radiation fluxes) were extracted from the National Centers for Environmental Prediction (NCEP)–National Center for Atmospheric Research (NCAR) reanalysis dataset from 1948 to the present (Kalnay et al. 1996; <ftp://ftp.cdc.noaa.gov/Datasets/>). The atmospheric fields from NCEP-NCAR dataset have a horizontal resolution of  $2.5^\circ \times 2.5^\circ$  and the surface heat fluxes data are on T62 Gaussian grids. This study also uses the monthly mean SAT data provided by the University of Delaware (Matsuura and Willmott 2009; <https://www.esrl.noaa.gov/psd/data/>). This SAT dataset is on a regular  $0.5^\circ$  latitude–longitude grid from 1901 to 2014.

Statistical significances of the regression and correlation coefficients are estimated based on the two-tailed Student's  $t$  test. The present study focuses on the variations on the inter-annual timescale. Hence, all the variables are subjected to a 9-year high pass Lanczos filter to obtain their interannual components (Duchon 1979), unless otherwise stated. The number of weights is nine for the 9-year high pass Lanczos filter. In addition, the reflective (symmetric) conditions are utilized in processing the start and end points of a time series. The results obtained in this study are similar when using the 7- or 11-year high pass Lanczos filter (not shown).

Wave activity flux proposed by Takaya and Nakamura (1997, 2001) was employed to examine propagation of the stationary Rossby waves. The wave activity flux is parallel to the local group velocity corresponding to a stationary wave train in the Wentzel–Kramers–Brillouin approximation and is independent of the wave phase (Takaya and Nakamura 1997, 2001). Equation of the wave activity flux is as follows:

$$W = \frac{p}{2|\bar{U}|} \left\{ \begin{array}{l} U(v'^2 - \psi'v'_x) + V(-u'v' + \psi'u'_x) \\ U(-u'v' + \psi'u'_x) + V(u'^2 + \psi'u'_y) \\ \frac{f_o R_a}{N^2 H_o} [U(v'T' - \psi'T'_x) + V(-u'T' - \psi'T'_y)] \end{array} \right\} \quad (1)$$

where  $H_o$ ,  $p$ ,  $T'$ ,  $R_a$ ,  $N$ , and  $f_o$  represent the scale height, pressure standardized by 1000 hPa, perturbed air temperature, gas constant related to dry air, and the Brunt–Vaisala frequency, and the Coriolis parameter at  $45^\circ\text{N}$ , respectively.  $\bar{U} = (U, V)$ ,  $\psi'$ , and  $\bar{V}' = (u', v')$  represent the mean winds, perturbed geostrophic stream function, and perturbed geostrophic winds, respectively. The subscripts  $x$  and  $y$  represents the derivatives in the zonal and meridional directions, respectively. In this study, climatological mean flow is calculated according to the period 1979–2014.

According to Holton (1992), in the spherical coordinate the horizontal surface temperature advection ( $T_{adv}$ ) can be written as follows:

$$T_{adv} = -u \frac{\partial T}{r \cos \varphi \partial \lambda} - v \frac{\partial T}{r \partial \varphi} \quad (2)$$

where  $\lambda$ ,  $\varphi$ ,  $r$ ,  $T$ ,  $u$  and  $v$  denote longitude, latitude, the radius of Earth, surface temperature, surface zonal and meridional winds, respectively. In Eq. (2), the terms on the right represent horizontal zonal and meridional advectons, respectively, from left to right. To further investigate the dominant horizontal advection processes, according to the linear perturbation theory, the horizontal zonal and meridional surface temperature advection anomalies could be decomposed as follows:

$$\left( -u \frac{\partial T}{r \cos \varphi \partial \lambda} \right)' = -\bar{u} \frac{\partial T'}{r \cos \varphi \partial \lambda} - u' \frac{\partial \bar{T}}{r \cos \varphi \partial \lambda} - u' \frac{\partial T'}{r \cos \varphi \partial \lambda} \quad (3)$$

$$\left( -v \frac{\partial T}{r \partial \varphi} \right)' = -\bar{v} \frac{\partial T'}{r \partial \varphi} - v' \frac{\partial \bar{T}}{r \partial \varphi} - v' \frac{\partial T'}{r \partial \varphi} \quad (4)$$

here, ( $'$ ) represents the anomalies.  $T'$ ,  $v'$ , and  $u'$  indicate anomalies of surface temperature, surface meridional and zonal winds, respectively.  $\bar{T}$ ,  $\bar{v}$ , and  $\bar{u}$  denote climatology of surface temperature, meridional and zonal winds, respectively. In Eq. (3), the left represents zonal temperature advection anomalies. The terms on the right indicate the zonal temperature advection anomalies induced by the zonal gradient of the temperature perturbation ( $-\bar{u} \frac{\partial T'}{r \cos \varphi \partial \lambda}$ ), zonal wind perturbation ( $-u' \frac{\partial \bar{T}}{r \cos \varphi \partial \lambda}$ ), and the higher-order zonal perturbations ( $-u' \frac{\partial T'}{r \cos \varphi \partial \lambda}$ ), respectively, from left to right.

In Eq. (4), the left is meridional temperature advection. The terms on the right denote the meridional temperature advection anomalies contributed by meridional gradient of the temperature perturbation ( $-\bar{v} \frac{\partial T'}{r \partial \varphi}$ ), meridional wind perturbation ( $-v' \frac{\partial \bar{T}}{r \partial \varphi}$ ), and the higher-order meridional perturbations ( $-v' \frac{\partial T'}{r \partial \varphi}$ ), respectively, from left to right.

### 3 Leading modes of winter Southeast Asian SAT variations

We first examine climatology and standard deviation of the Southeast Asian original SAT during boreal winter (DJF-averaged). Following Zveryaev and Aleksandrova (2004), the region for Southeast Asia we choose for analysis extends from  $8^\circ$  to  $32^\circ\text{N}$  and from  $94^\circ$  to  $123^\circ\text{E}$ . The results obtained

in this study are not sensitive to the reasonable change of the selected region. Figure 1a, b displays the climatology and standard deviation of winter original SAT over Southeast Asian region during 1979–2014, respectively. High climatological winter mean SAT appears over the south part of Indo-China Peninsula and the Luzon island, and gradually decreases northward (Fig. 1a). Large standard deviation of winter SAT occurs over northeast part of Indo-China Peninsula and the south China (Fig. 1b). Small standard deviation of SAT occurs over the Luzon island and the south coast of Indo-China Peninsula (Fig. 1b). As this study analyzes the SAT variation on the interannual timescale, the percent SAT variance explained by its interannual component over Southeast Asian region is examined in Fig. 1c. It is found that the interannual component of SAT anomalies can explain above 70% of original SAT anomalies over most parts of the Southeast Asia. In particular, SAT interannual anomalies over the Luzon Island and the regions extending from central Indo-China Peninsula northward to south China explain around 85% of the original SAT variations (Fig. 1c).

We further extract the dominant modes of winter SAT interannual variations over Southeast Asia for the period 1979–2014 via using an EOF method. To account for the change in the area in different latitude, SAT interannual anomalies were weighted by cosine of the latitude before EOF analysis (North et al. 1982a). Figure 2a, b display spatial distribution of SAT anomalies related to the first and second EOF modes (EOF1 and EOF2), respectively. EOF1 and EOF2 explain 53.5 and 23.9% of the total SAT variance, respectively. According to the criterion proposed by North et al. (1982b), the first two EOF modes are well separated from each other and from the remainder of the EOF modes. EOF1 is featured by a consistent cooling (warming) pattern over Southeast Asia, with relatively large loading over the northeast part of Indo-China Peninsula and the south China (Fig. 2a). Spatial distribution of the EOF1 is similar to the spatial pattern of the standard deviation of SAT variation (Figs. 1b, 2a). The EOF2 displays a dipole pattern, with opposite SAT variation between the Indo-China Peninsula and the south China (Fig. 2b). The principal component (PC) time series corresponding to EOF1 and EOF2 show obvious interannual variations (Fig. 2c, d).

We have checked the first two EOF modes of the southeast Asian SAT interannual variations based on reasonable changes of the selected domains (e.g.,  $5^{\circ}$ – $35^{\circ}$ N and  $96^{\circ}$ – $122^{\circ}$ E,  $8^{\circ}$ – $30^{\circ}$ N and  $95^{\circ}$ – $120^{\circ}$ E, and  $10^{\circ}$ – $33^{\circ}$ N and  $97^{\circ}$ – $121^{\circ}$ E). It is found that the SAT anomalies over the Southeast Asia related to the EOF1 and EOF2 are very similar (not shown). In addition, the correlation coefficients among the PC time series of the EOF1 (EOF2) based on different domains are larger than 0.99 (0.96), significant at the 99.9% confidence level based on the two-tailed Student's *t* test. This implies that the results obtained in this study

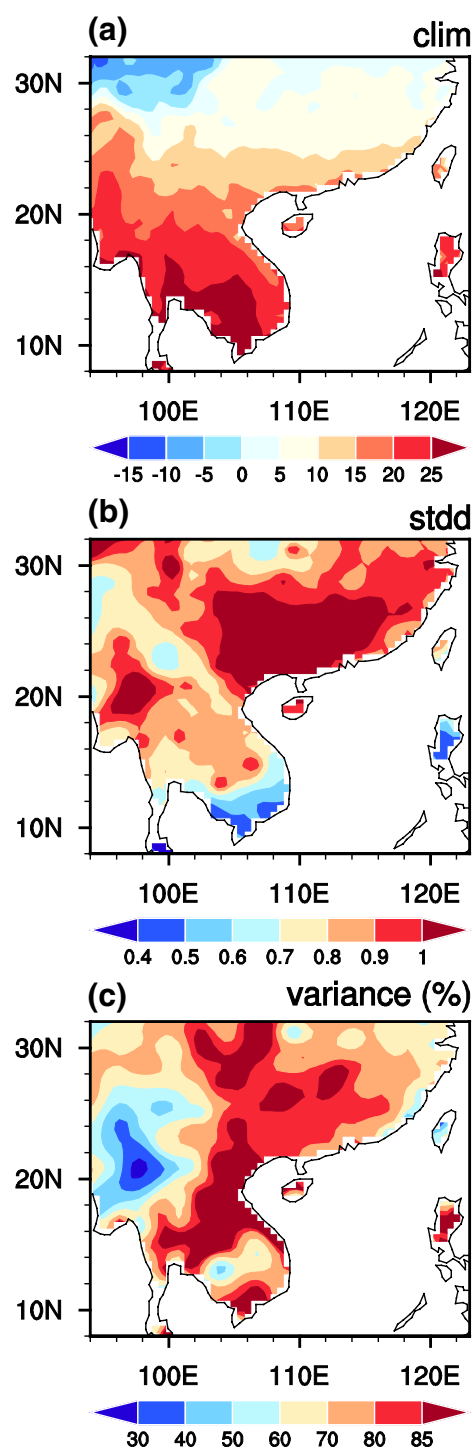


**Fig. 1** **a** Climatology (unit:  $^{\circ}$ C) and **b** standard deviation (unit:  $^{\circ}$ C) of boreal winter (DJF-averaged) surface air temperature (SAT) over Southeast Asian region during 1979–2013. **c** Percentage of variance (unit: %) of winter SAT variations over Southeast Asia during 1979–2014 explained by its interannual component

are not sensitive to the reasonable changes of the selected regions. In addition, we have also examined the EOF results based on the original SAT data (not shown). It is found that

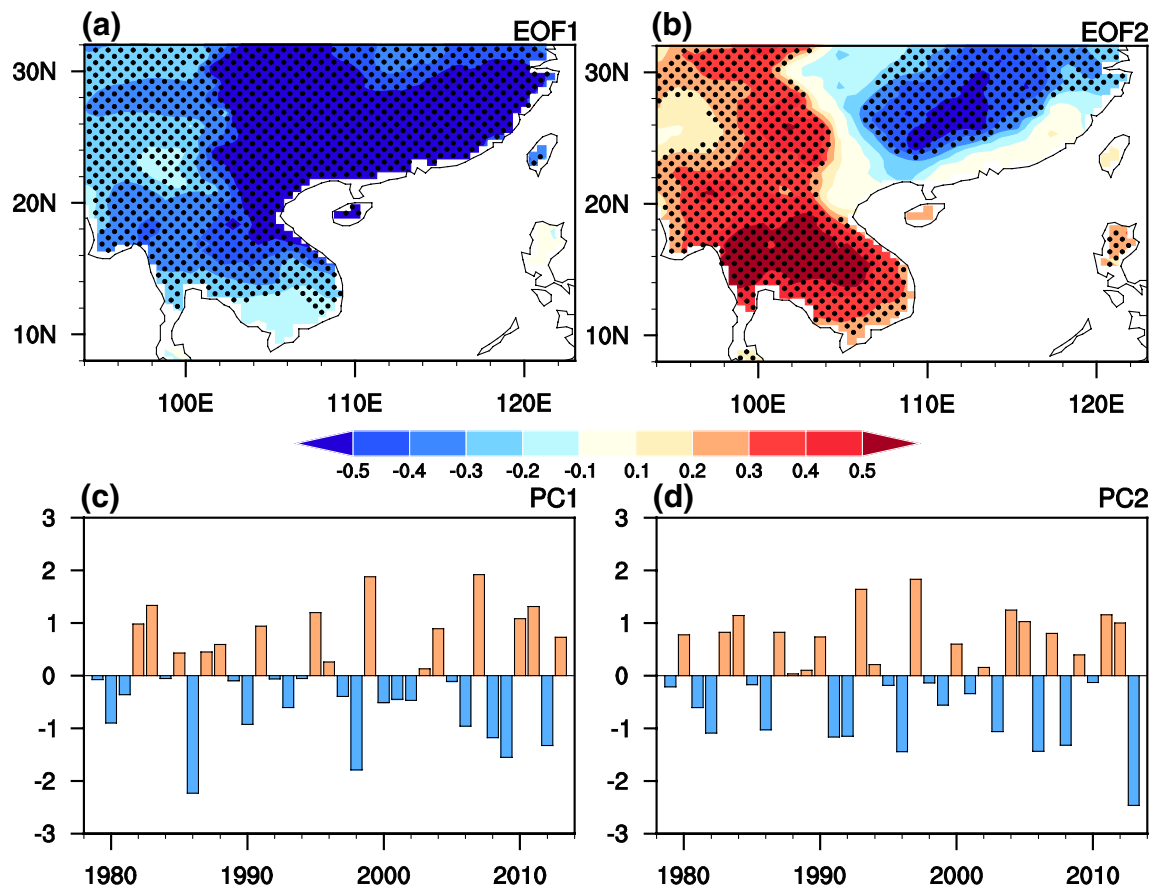


**Fig. 2** Winter SAT ( $^{\circ}\text{C}$ ) anomalies obtained by regression upon the normalized PC times series corresponding to **a** EOF1 and **b** EOF2 of Southeast Asian winter SAT interannual anomalies during 1979–2014. **c**, **d** The normalized PC time series corresponding to EOF1 and

EOF2 of Southeast Asian SAT, respectively. Stippling in **a**, **b** denotes SAT anomalies that are significantly different from zero at the 95% confidence level according to the two-tailed Student's *t* test

spatial structures of the first two EOF modes of the original SAT variations over the Southeast Asia are similar to those based on the 9-year high pass filtered SAT anomalies. This implies that the SAT anomaly patterns in EOF1 and EOF2 are common to both interannual variation and long-term trends. However, the corresponding PC time series of the first two EOF modes based on the original data both display notable long-term linear trends (significant at the 95% confidence level). As the factors responsible for the SAT anomalies over the Southeast Asia on different timescale (e.g., interannual, interdecadal and long-term trend) may be different, this study only focuses on investigating the SAT variations on the interannual timescale. Interdecadal variation and long-term trend of the Southeast Asian SAT anomalies and the related factors would be investigated in the future.

Power spectra of the PC time series corresponding to EOF1 and EOF2 are shown in Fig. 3 to examine their dominant frequencies. The 95% upper confidence limit of the white noise spectrum is also shown to examine the

significance of the spectrum (represented by the blue line in Fig. 3). The 95% upper confidence limit of white noise spectrum is calculated from the white noise spectrum according to the Chi square ( $\chi^2$ ) distribution at the 95% confidence level (Huang 2004). The PC1 time series shows a significant spectral peak around 4 year (Fig. 3a). In contrast, the PC2 time series captures two notable spectral peaks around 2.5 year and 3.6 year (Fig. 3b).

## 4 Factors for the Southeast Asian SAT variations related EOF1 and EOF2

### 4.1 Surface heat flux changes

To understand formation of SAT anomalies related to the first two EOF modes of winter Southeast Asian SAT, we first check change in the surface heat fluxes. In the following analysis, values of surface heat fluxes are negative (positive) when they are upward (downward), acting to cool (warm) the

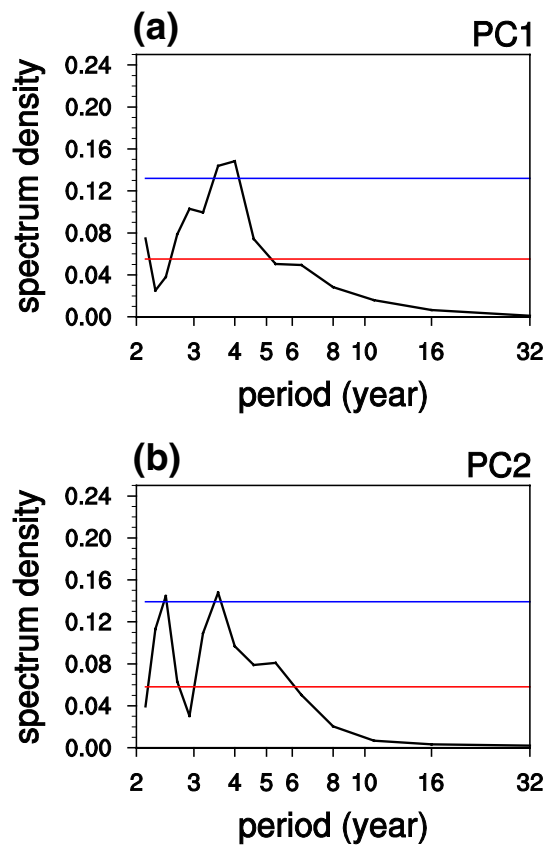


**Fig. 3** Power spectrum (black line) of the normalized PC time series corresponding to EOF1 and EOF2 of Southeast Asian winter SAT anomalies. Red and blue lines in **a**, **b** represent the white noises spectra and the corresponding 95% confidence upper limit, respectively

surface. Figures 4 and 5 shows anomalies of winter surface net heat flux, surface shortwave and longwave radiations, surface sensible and latent heat fluxes obtained by regression upon the normalized PC time series corresponding to the EOF1 and EOF2, respectively.

For the EOF1, surface net heat flux anomalies are insignificant over Southeast Asian region (Fig. 4a). This indicates that SAT anomalies related to EOF1 over Southeast Asia cannot be explained by the surface heat flux change (Figs. 2a, 4a). Insignificant change in the surface net heat flux is due to the opposite changes of surface shortwave radiation and latent heat flux with the surface longwave radiation and sensible heat flux (Fig. 4b–e). In particular, increases in the surface shortwave radiation and latent heat flux are apparent in the south China and the Indo-China Peninsula (Fig. 4b, e). By contrast, the surface longwave radiation and sensible heat flux anomalies display significant decrease in the above regions (Fig. 4c, d). Increase in the surface shortwave radiation and decrease in the surface longwave radiation in the south China and the Indo-China Peninsula may be partly related to the decrease in the total cloud cover

(Figs. 4b, c, 6a). As demonstrated by previous study (Chen et al. 2016a; Chen and Wu 2017), less cloud cover tends to lead to more (less) shortwave (longwave) radiation reaching the surface.

For the EOF2 of winter Southeast Asian SAT, spatial distribution of surface net heat flux anomalies (Fig. 5a) bears some resemblances to that of SAT changes (Fig. 2b), with significant positive anomalies over the Indo-China Peninsula and pronounced negative anomalies over the south China. This indicates that formation of the SAT anomalies related to EOF2 can be partly attributed to the change in the surface net heat flux. Over the south China region, decrease in the surface shortwave radiation is the primary contributor to the net surface heat flux change (Fig. 5a, b). Surface latent heat flux change also has a positive contribution to the net surface heat flux decrease (Fig. 5a, e). By contrast, change in the surface longwave radiation has a negative contribution to the net surface heat flux change (Fig. 5a, c). Surface sensible heat flux anomalies over the south China are relatively weak and cannot pass the 95% confidence level according to the two-tailed Student's *t* test (Fig. 5d). Over the Indo-China Peninsula, increase in the net surface heat flux is mainly attributed to increase in the surface longwave radiation (Fig. 5a, c). In comparison, change in the surface shortwave radiation contributes negatively to the net heat flux change (Fig. 5a, c). In addition, surface sensible and latent heat flux changes are weak and insignificant in the Indo-China Peninsula (Fig. 5d, e). Again, it seems that change in the surface shortwave and longwave radiation related to the EOF2 may be related to the changes in the total cloud cover (Figs. 5b, c, 6b). In particular, increase in the total cloud cover would reflect more downward shortwave radiation, resulting in less downward shortwave radiation reaching the surface and hence a smaller surface shortwave radiation. By contrast, more upward longwave radiations would be reflected back into the surface when more total cloud cover appears. Hence, this leads to an increase in the surface longwave radiation (Chen et al. 2016a; Chen and Wu 2017). The reverse conditions are true for decrease in the total cloud cover.

#### 4.2 Atmospheric circulation anomalies related to EOF1 and EOF2

Above analysis shows that change in the SAT over Southeast Asia related to EOF1 cannot be explained by the surface net heat flux change. In addition, surface net heat flux anomalies only partly explain the SAT anomalies related to EOF2. These evidences suggest that atmospheric circulation changes may play an important role in the SAT anomalies. In the following, we further check the atmospheric circulation anomalies related to EOF1 and EOF2 of Southeast Asian SAT variation.

**Fig. 4** Anomalies (unit:  $W m^{-2}$ ) of winter surface **a** net heat flux, **b** shortwave radiation, **c** longwave radiation, **d** sensible heat flux, and **e** latent heat flux regressed upon the normalized PC time series corresponding to EOF1 of winter Southeast Asian SAT variations. Stippling in **a–e** denotes anomalies that are significantly different from zero at the 95% confidence level

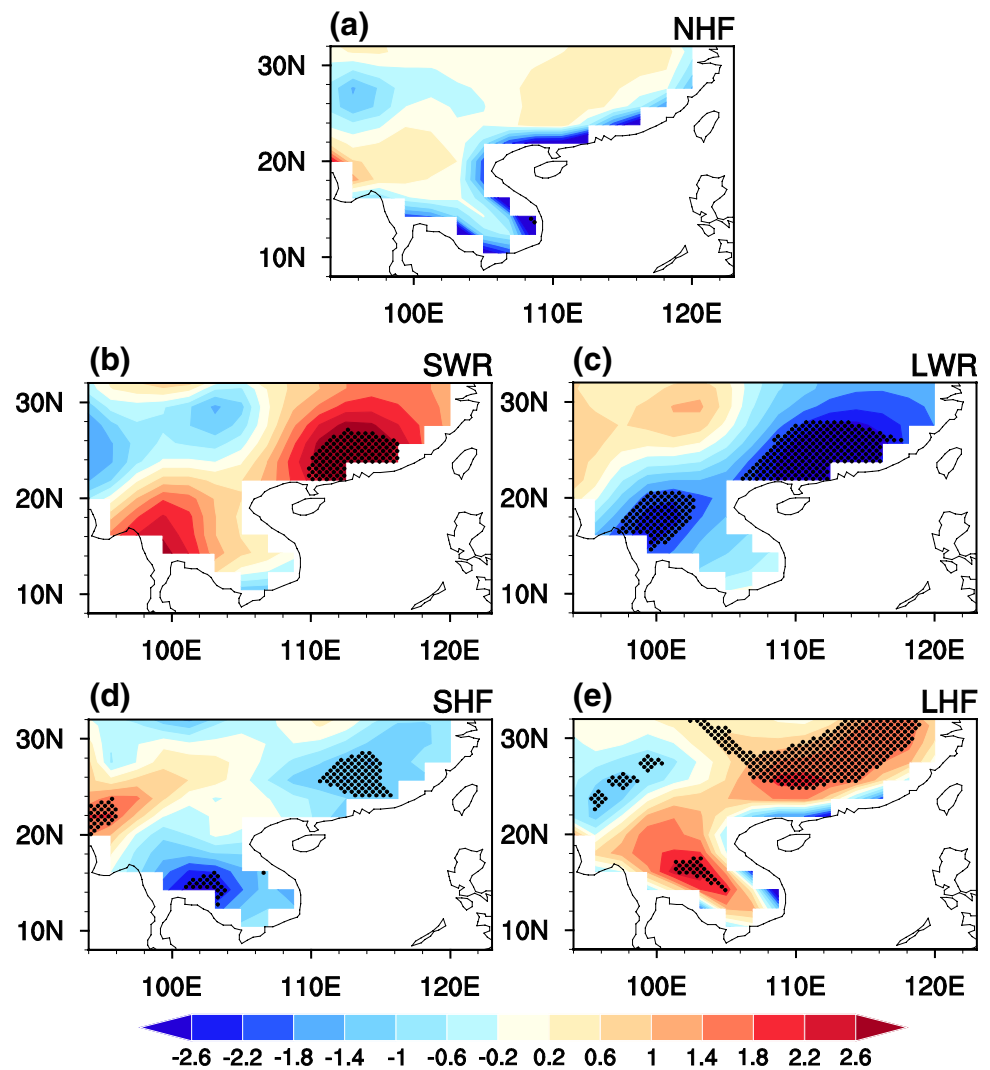
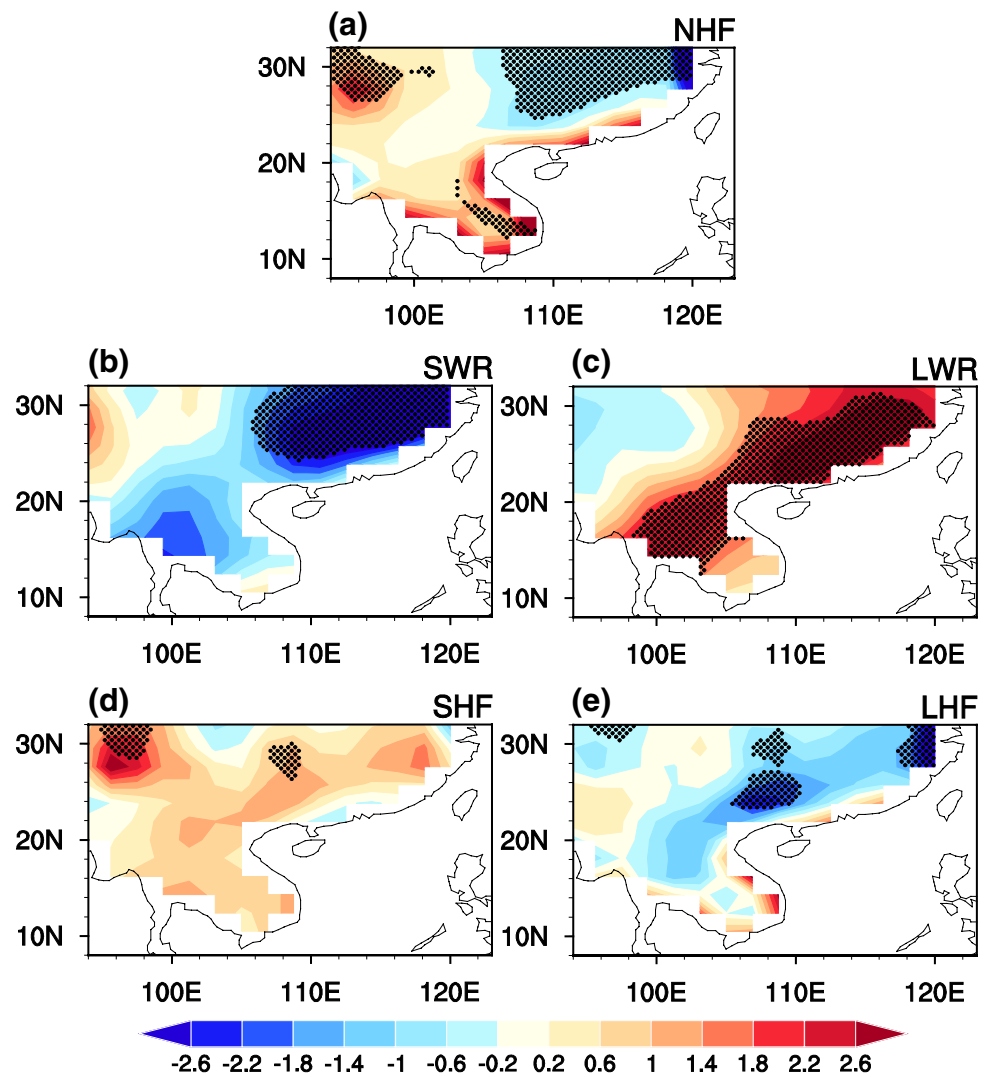


Figure 7a, b display winter 1000 hPa winds and stream function anomalies obtained by regression upon the normalized PC time series corresponding to EOF1 and EOF2, respectively. It is found that spatial distributions of 1000 hPa winds anomalies correspond well to the patterns of SAT changes related to EOF1 and EOF2 (Figs. 2a, b, 7a, b). For the EOF1, an anomalous cyclone (related to a center of negative stream function anomaly) occurs around the South China Sea and the Philippines, accompanied with pronounced northerly wind anomalies over East China extending southward to Southeast Asia (Fig. 7a). These significant anomalous northerly winds may explain generation of the negative SAT anomalies over Southeast Asia via carrying colder air from higher latitudes (Figs. 2a, 7a). For the EOF2, significant northerly wind anomalies appear over the south China (Fig. 7b), which may be associated with a large-scale anomalous anticyclone over mid-latitude Eurasia. These anomalous northerly winds may explain formation of the negative SAT anomalies via wind induced

temperature advection (Figs. 2b, 7b). In addition, a pair of cyclonic anomaly is observed over the tropical north and south Indian Ocean, leading to significant southerly wind anomalies observed over the Indo-China Peninsula, which contribute to positive SAT anomalies there (Figs. 2b, 7b). Formation of these two cyclonic anomalies over the tropical north and south Indian Ocean may be related to the Gill-type atmospheric response to the positive SST anomalies over the tropical Indian Ocean, which would be further analyzed in Sect. 4.3. Note that formation of the southerly wind anomalies over the Indo-China Peninsula may also be attributed to the cross-equatorial flow over the South China Sea (Fig. 7b).

Above analysis suggests that formations of the SAT anomalies over the Southeast Asia related to EOF1 and EOF2 may be mainly via temperature advection induced by the atmospheric circulation changes. To confirm this assertion, the horizontal zonal and meridional surface temperature advections are calculated (Eq. (2)). Figure 8 displays anomalies of winter zonal and meridional temperature

**Fig. 5** As in Fig. 4, but for surface heat flux anomalies regressed upon the normalized PC time series corresponding to EOF2 of winter Southeast Asian SAT variations



advectations obtained by regression upon the normalized PC time series of the first two EOFs of winter Southeast Asian SAT variations. For the EOF1, the significant negative SAT anomalies over the Indo-China Peninsula and the south China are mainly attributed to the cold meridional temperature advection (Figs. 2a, 8c). Formations of the negative SAT anomalies over the Indo-China Peninsula related to the EOF1 are also partly attributed to the cold zonal temperature advection (Figs. 2a, 8a). By contrast, the warm zonal temperature advection contributes negatively to the negative SAT anomalies over the south China related to the EOF1 (Figs. 2a, 8a). For the EOF2, the meridional temperature advection anomalies display a dipole anomaly pattern, with positive anomalies over the Indo-China Peninsula and negative anomalies over the south China, similar to the horizontal structure of the SAT anomalies related to the EOF2 (Figs. 2b, 8d). In addition, it is noted that the warm (cold) zonal temperature advection anomalies over the south China (Indo-China Peninsula) contribute negatively to the negative

SAT anomalies there related to the EOF2 (Figs. 2b, 8b). Above results indicates that formation of the SAT anomalies over the south China and the Indo-China Peninsula related to the first two EOF modes are mainly attributed to the meridional temperature advection.

To examine which components of the horizontal temperature advection is crucial in contributing to the SAT anomalies, we further check different components of the horizontal temperature advectations (Eqs. (3) and (4)) related to the EOF1 in Fig. 9 and those related to the EOF2 in Fig. 10. For the EOF1, regarding the meridional temperature advection induced by the meridional wind anomalies is the dominant factor in contributing to the formation of the negative SAT anomalies over the south China and the Indo-China Peninsula (Figs. 2a, 9d). It is noted that the anomalous wind-generated meridional temperature advection is resulted from the significant northerly wind anomalies over the Southeast Asia as shown in Fig. 7a. In addition, the anomalous meridional



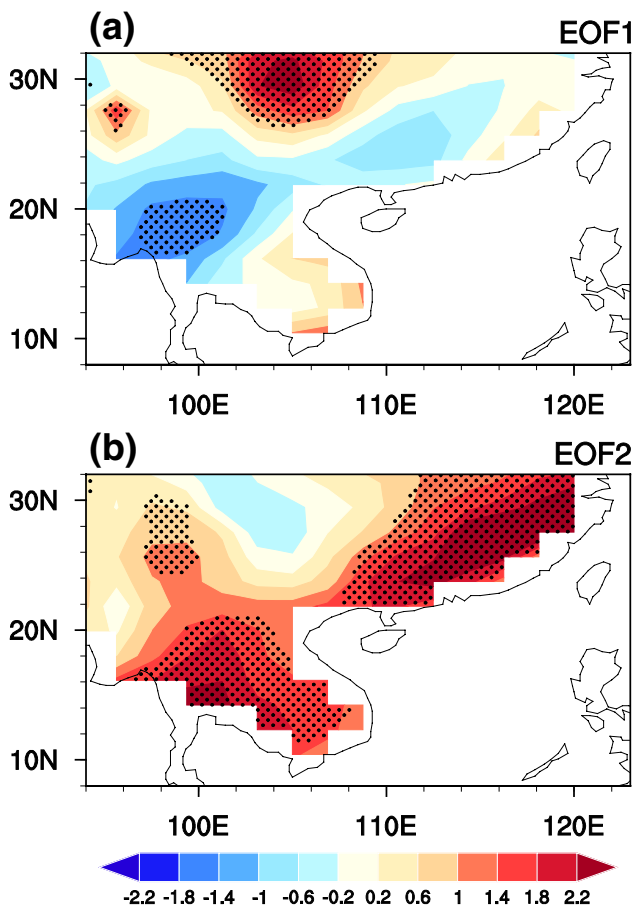


**Fig. 6** Anomalies (unit: %) of winter total cloud cover regressed upon the normalized PC time series corresponding to **a** EOF1 and **b** EOF2 of winter Southeast Asian SAT variations. Stippling in **a**, **b** denotes anomalies that are significantly different from zero at the 95% confidence level

temperature advection due to the meridional gradient of the surface temperature also partly positively contribute to the negative SAT anomalies over the Indo-China Peninsula and south coast of south China (Fig. 9e). The higher-order meridional perturbations have a weak contribution to the SAT anomalies over the Southeast Asia related to the EOF1 (Fig. 9e). Regarding the zonal temperature advection, the advection induced by the zonal gradient of the surface temperature contribute negatively (positively) to the SAT anomalies over the south China (Indo-China Peninsula) (Fig. 9b). In addition, the zonal temperature advection induced by the zonal wind perturbation (Fig. 9a) and higher-order zonal wind perturbation (Fig. 9c) are relatively weak and less insignificant. Above evidences indicates that the horizontal temperature advection induced by the meridional wind perturbation plays a dominant role in the formation of the SAT anomalies over the Southeast Asia related to the EOF1.

For the EOF2, regarding the meridional temperature advection, again, it is clear that the advection induced by

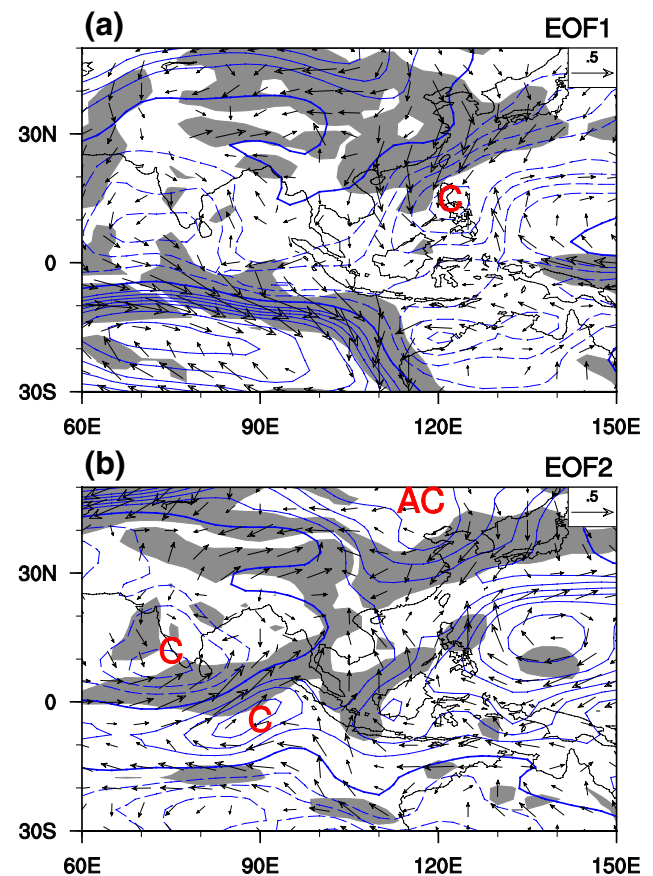


**Fig. 7** Anomalies of 1000 hPa winter winds (vector, unit:  $\text{m s}^{-1}$ ) and stream function (contours, unit:  $10^5 \text{ m}^2 \text{ s}^{-1}$ ) regressed upon the normalized PC time series corresponding to **a** EOF1 and **b** EOF2 of winter Southeast Asian SAT variations. The shading in **a**, **b** denotes regions where either component of the wind anomalies that is significantly different from zero at the 95% confidence level. Contour intervals are  $0.5 \times 10^5 \text{ m}^2 \text{ s}^{-1}$  and zero lines are in bold in **a** and **b**. Negative (positive) values of stream function are indicated by blue dashed (solid) lines in **a**, **b**

the meridional wind perturbation plays a crucial role in contributing to the formation of the dipole SAT anomalies over the southeast Asia (Fig. 10d). The meridional advection induced by the meridional gradient of surface temperature also positively contributes to the negative SAT anomalies over the south China (Fig. 10e). The meridional advection due to the high-order meridional perturbations is relatively weak (Fig. 10f). Regarding the zonal temperature advection, the advection induced by the zonal wind perturbation is less organized and less significant over the south China and Indo-China Peninsula (Fig. 10a). The zonal advection resulted from the zonal gradient of the surface temperature also displays a dipole structure, but with signs opposite to the SAT anomalies (Fig. 10b), contributing negatively to the SAT anomalies related to the EOF2 over the south China and the Indo-China Peninsula (Fig. 10b). The higher-order zonal perturbations are weak (Fig. 10c). Hence, similar to

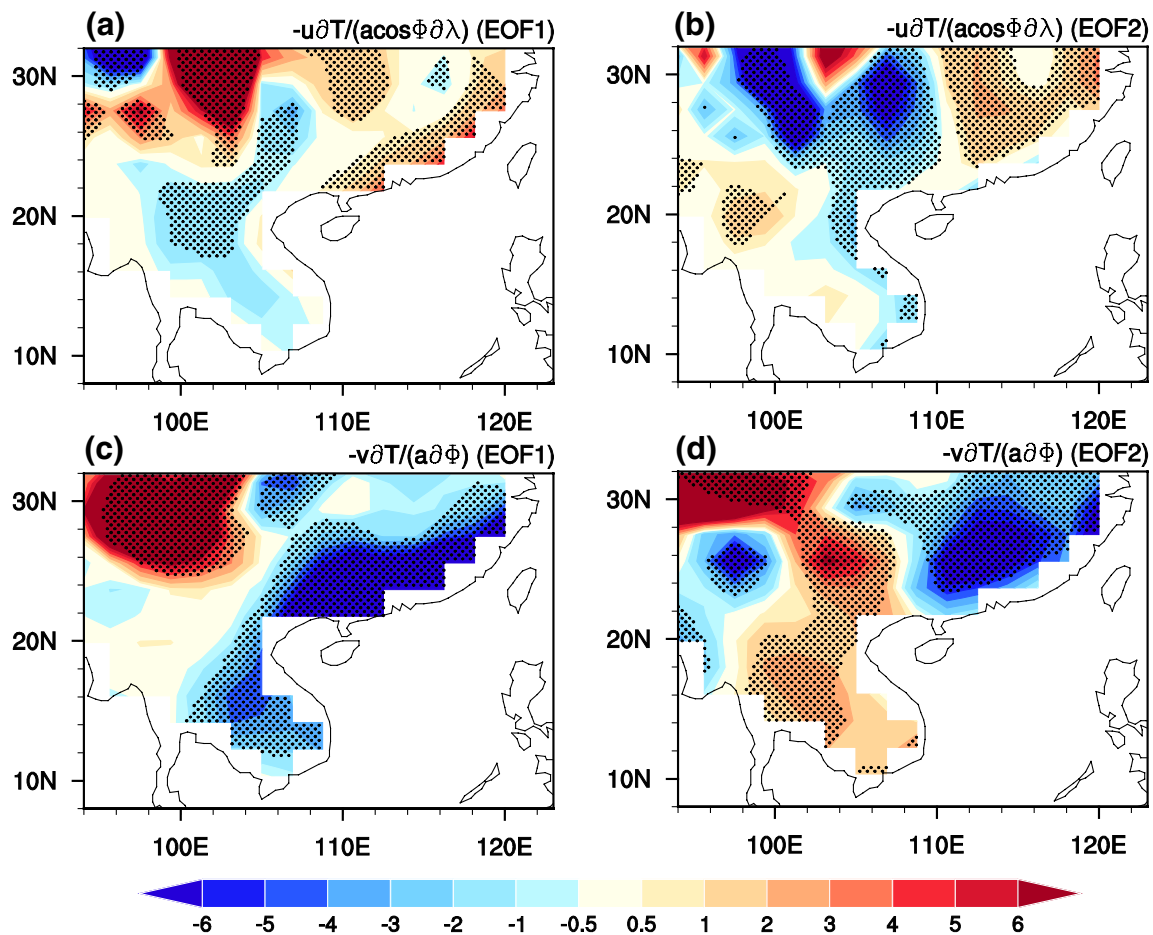


**Fig. 8** Anomalies (unit:  $^{\circ}\text{C } 3 \text{ month}^{-1}$ ) of winter surface air temperature **a, b** zonal advection and **c, d** meridional advection regressed upon the normalized PC time series corresponding to (left column)

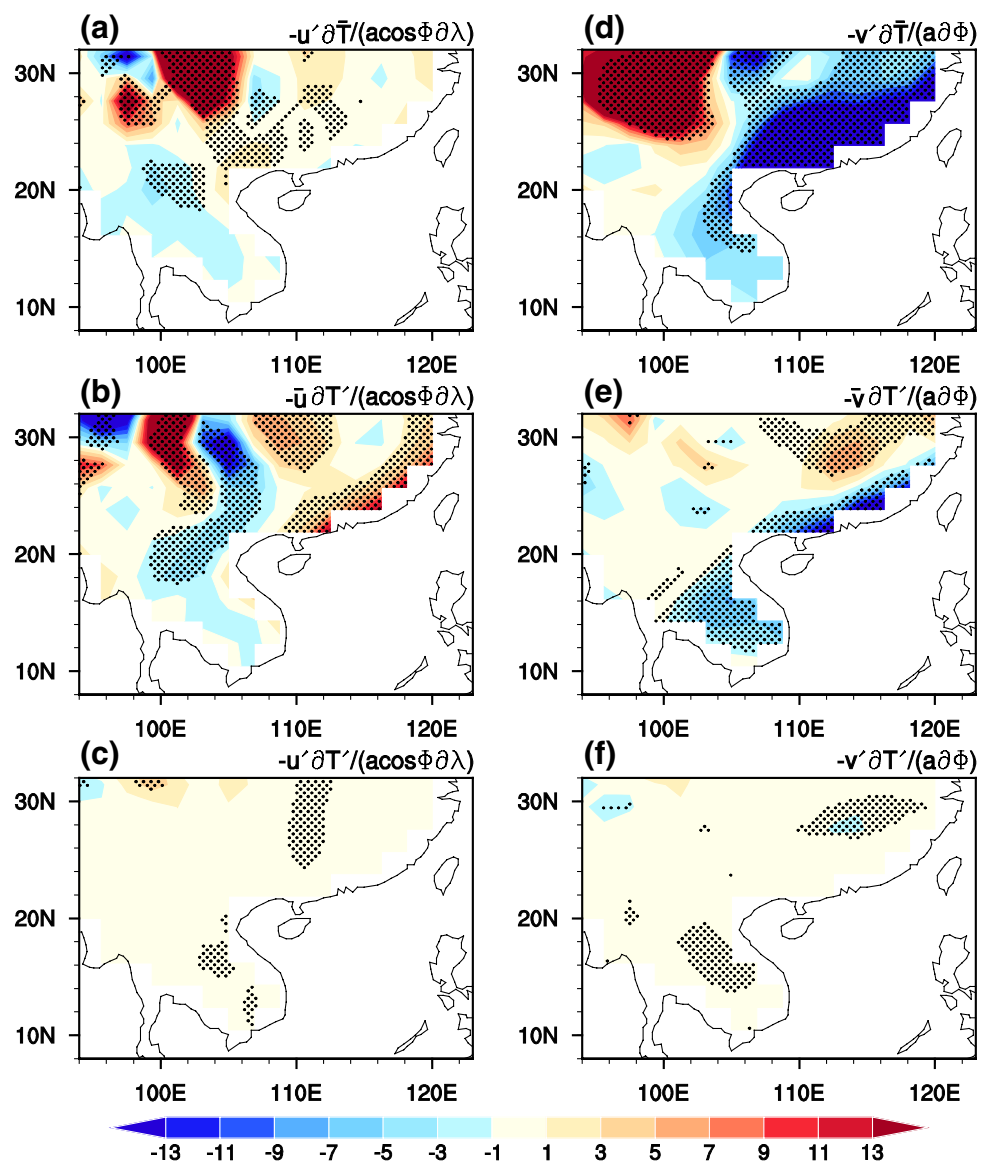
EOF1 and (right column) EOF2 of winter Southeast Asian SAT variations. Stippling in **a–d** denotes anomalies that are significantly different from zero at the 95% confidence level

EOF1, the horizontal advection induced by the meridional wind anomalies plays a key role in the formation of the SAT anomalies related to the EOF2. These results also further confirm the important role of the atmospheric circulation changes for the formations of the SAT anomalies related to EOF1 and EOF2 of the winter Southeast Asian SAT interannual variations.

In the following, we further examine the possible factors responsible for the generations of the atmospheric circulation changes related to the EOF1 and EOF2 of the Southeast Asian winter SAT variations. From Fig. 7, it seems that atmospheric circulation anomalies associated with the EOF1 and EOF2 are originated from the regions beyond Southeast Asia. Figure 11 displays winter SLP and 200 hPa geopotential height anomalies obtained by regression upon the normalized PC time series of the first two EOF modes, respectively. For the EOF1, significant negative SLP and 200 hPa geopotential height anomalies are seen over large parts of the tropical Ocean regions (Fig. 11a, b). These may be induced by the La Niña-like SST anomalies over the

tropical central-eastern Pacific, which would be discussed in Sect. 4.3. Over the mid-high latitudes of Northern Hemisphere, SLP and geopotential height anomalies show a clear meridional dipole anomaly pattern, with significant negative anomalies over high latitudes and positive anomalies over mid-latitudes (Fig. 11a, b). The spatial distribution of atmospheric circulation anomalies over the mid-high latitudes bear a resemblance to that related to the positive phase of the AO (Thompson and Wallace 1998, 2000; Cheung et al. 2012; Chen et al. 2014a, b, 2015). Specifically, the correlation coefficient between PC1 of winter Southeast Asia SAT and the winter AO index reaches  $-0.42$ , significant at the 95% confidence level according to the Student's  $t$  test. Here, following previous studies (Thompson and Wallace 1998; Chen et al. 2014a, b), the AO index is defined as the PC time series corresponding to EOF1 of SLP anomalies north of  $20^{\circ}\text{N}$ . This implies that the winter AO may have a close connection with the EOF1 of the winter Southeast Asian SAT variations. To further confirm role of the winter AO in influencing the SAT anomalies over the Southeast Asia, we

**Fig. 9** Anomalies (unit:  $^{\circ}\text{C}$   $3 \text{ month}^{-1}$ ) of six components of winter horizontal SAT advection obtained by regression upon the normalized PC time series corresponding to EOF1 of winter Southeast Asian SAT variations. Stippling in the figures denotes anomalies that are significantly different from zero at the 95% confidence level

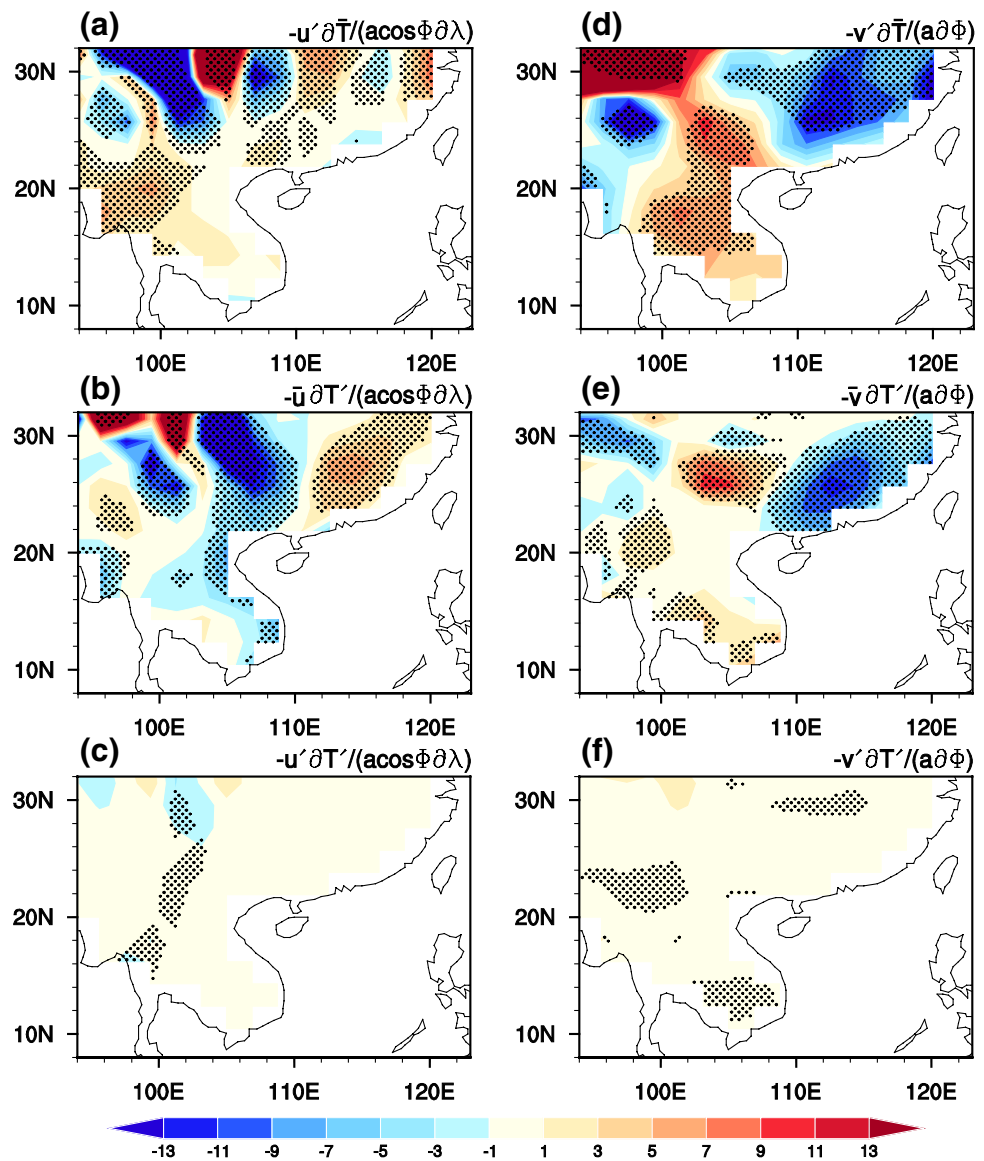


display 1000 hPa wind anomalies obtained by regression upon the winter AO index in Fig. 12a. It is found that significant northerly wind anomalies are observed around the Southeast Asia. The northerly wind anomalies induced by the winter AO may contribute to the formation of the negative SAT anomalies there. The detailed physical process for the formation of the northerly wind anomalies around the Southeast Asia induced by the winter AO remains unclear at present, which would be further investigated. It is noted that previous studies have demonstrated that SAT anomalies are positive (negative) over many parts of the mid-high latitudes of Eurasia (including East Asia) during the positive (negative) phase of the winter AO (Thompson and Wallace 1998, 2000; Gong et al. 2001; Jeong and Ho 2005; He and Wang 2016). However, in this study we found that SAT anomalies over Southeast Asia were positive (negative) during negative

(positive) phase of the wintertime AO. This indicates that impacts of the winter AO on the Southeast Asian SAT are different to those on the mid-high latitudes of Eurasia. Further analyses are needed to identify the factors responsible for the differences.

Furthermore, it is showed that significant positive SLP anomalies are observed over the Siberian High region. Siberian high is an important component of the East Asian winter monsoon (EAWM). The EAWM intensity would be stronger when the Siberian High enhanced. In addition, Ding (1987) indicated that occurrence of cold surge over East Asia was closely related to the Siberian High intensity. Zhang et al. (1997) showed that a certain intensity of the Siberian High is a crucial condition for the occurrence of East Asian cold surge. These suggest that generation of the significant northerly wind anomalies over East Asia and Southeast

**Fig. 10** As in Fig. 9, but for the anomalies of six components of winter horizontal SAT advection obtained by regression upon the normalized PC time series corresponding to EOF2 of winter Southeast Asian SAT variations



Asia (Fig. 7a) may be related to change in the Siberian High intensity. We have calculated the correlation coefficient between the Siberian High intensity index and the PC1 time series of winter Southeast Asian SAT, with the correlation coefficient being 0.5, which is significant at the 95% confidence level. Note that the Siberian High intensity index is defined as the area-averaged SLP anomalies over the region of 40°–60°N and 80°–120°E following the method proposed by Wu and Wang (2002). In addition, Fig. 12b displays wintertime 1000 hPa wind anomalies obtained by regression upon the normalized Siberian high intensity index. It is clear that significant northerly wind anomalies are found around the East Asia and extend southward to the Southeast Asia when the Siberian high strengthened (Fig. 12b). Spatial distribution of the 1000 hPa wind anomalies shown in Fig. 12b bear a close resemblance to that related to a stronger EAWM

(Chen et al. 2000). Hence, this implies that variation of the Siberian high can impact the southeast Asian SAT anomalies via modulating the EAWM intensity.

It is noted that previous studies have demonstrated that the wintertime AO may impact the East Asian SAT via modulating the Siberian high (e.g., Gong et al. 2001; Wu and Wang 2002). However, in the present study, we found that the correlation coefficient between the winter Siberian High intensity index and the winter AO index is only 0.13 during 1979–2013, which is weak and insignificant. This suggests that interannual variation of winter Siberian High intensity is independent of the winter AO during 1979–2014. Actually, a recent study showed that the connection between the Siberian high and the winter AO is unstable (Huang et al. 2016). The reason for the change in the connection of the Siberian high and the winter AO remains to be explored.

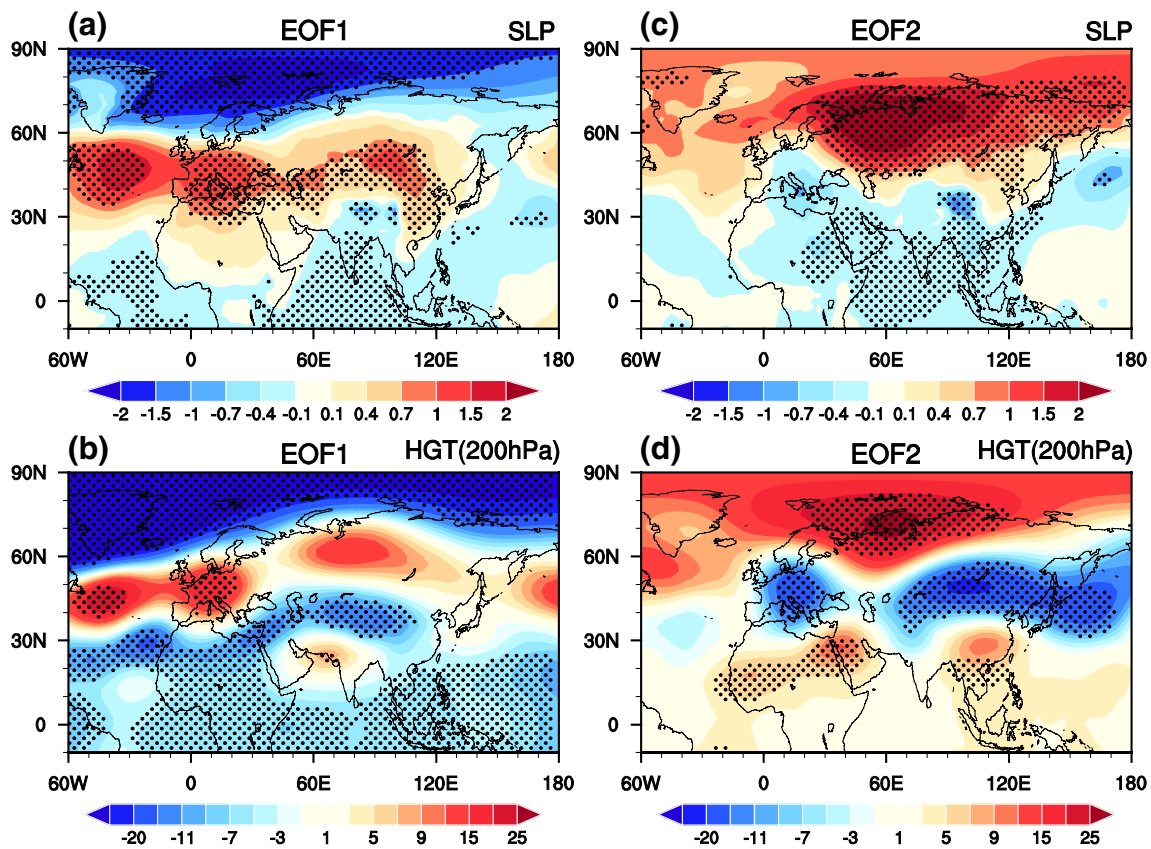


**Fig. 11** Anomalies of winter **a, b** SLP (unit: hPa) and **c, d** 200 hPa geopotential height (unit: gpm) regressed upon the normalized PC time series corresponding to (left column) EOF1 and (right column)

EOF2 of winter Southeast Asian SAT variations. Stippling in **a–d** denotes anomalies that are significantly different from zero at the 95% confidence level

Corresponding to the EOF2 mode, significant and positive SLP anomalies appear over the north part of Eurasian continent and pronounced negative SLP anomalies occur over the tropical Northern Indian Ocean (Fig. 11c). Formation of the negative SLP anomalies over the tropical Northern Indian Ocean may be due to the underlying SST warming anomalies, which will be discussed in the following sub-section. At 200 hPa, significant and negative geopotential height anomalies are observed over the Europe and around the Lake Baikal extending eastward to East Asia–North Pacific region (Fig. 11d). In addition, pronounced positive geopotential anomalies are seen over the north coast of Eurasia, North Africa, and Southeast Asia (Fig. 11d). Specifically, the significant positive 200 hPa geopotential height and associated anticyclonic circulation anomalies in the upper troposphere (not shown) may be related to the increase in the total cloud cover (Figs. 6b, 11d).

To help understand genesis of the significant positive geopotential height anomalies over Southeast Asia, we display winter 200 hPa wave activity flux and stream function anomalies obtained by regression upon the normalized PC time series corresponding to EOF2 of winter Southeast Asian

SAT variation in Fig. 13. Two atmospheric wave trains can be clearly observed (Fig. 13). A wave train extends around the Mediterranean Sea southeastward to the Middle East and then turns eastward to Southeast Asia (Fig. 13). This atmospheric wave train bear a close resemblance to that identified in Watanabe (2004), and Hu et al. (2017). Watanabe (2004) and Hu et al. (2017) showed that formation of this wave train is closely related to the upper-level convergence anomalies around the Mediterranean, and it can propagate firstly southeastward, and then eastward to East Asia along the wintertime Asian jet (Watanabe 2004; Hu et al. 2017). Furthermore, the atmospheric circulation anomalies related to this wave train have a large impact on the weather and climate anomalies over many parts of the East Asia (Hu et al. 2017). This study shows that SAT anomalies related to EOF2 of winter Southeast Asian SAT interannual variations may also be impacted by this atmospheric wave train.

Another wave train is observed around the Arctic Kara Sea extending southeastward to the Southeast Asia (Fig. 13). Formation of this wave train seems to be related to the Arctic sea ice change (SIC). Previous studies have demonstrated that change in the Arctic SIC can exert an influence on the

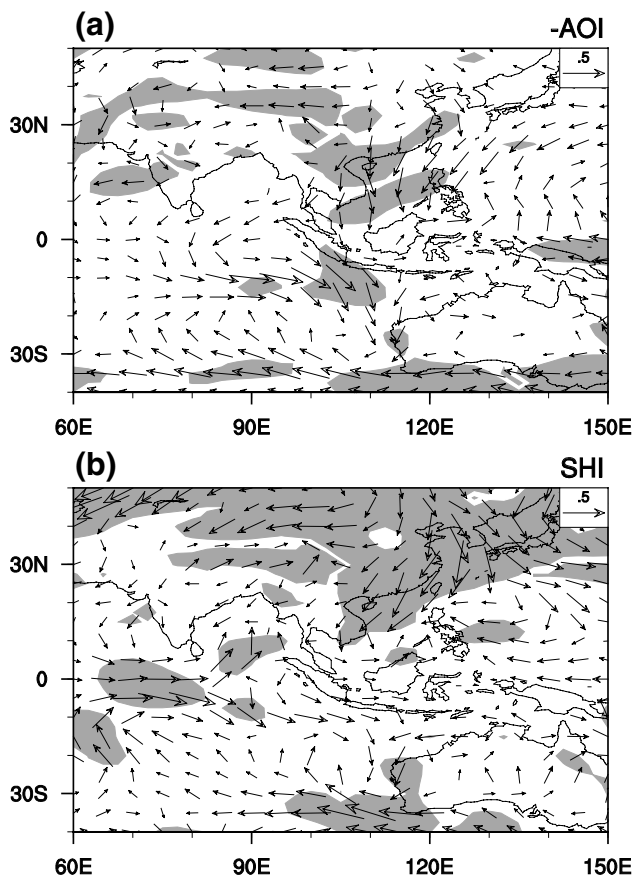


**Fig. 12** Anomalies of winter winds at 1000 hPa (unit:  $\text{m s}^{-1}$ ) regressed upon the winter **a** Siberian High index (SHI) and minus one Arctic Oscillation index (AOI). The shading in **a**, **b** denotes regions where either component of the wind anomalies that is significantly different from zero at the 95% confidence level

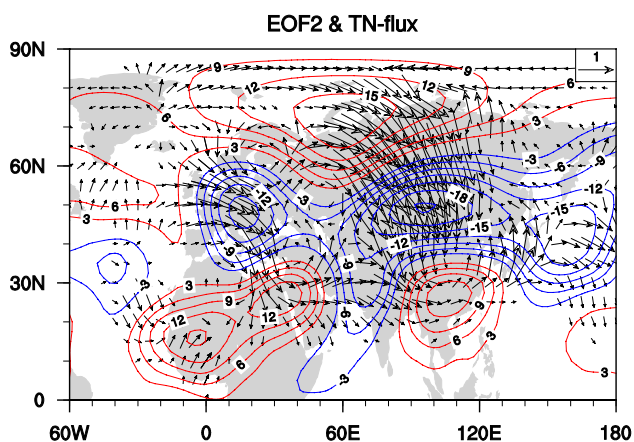


**Fig. 13** Anomalies of winter wave activity flux (vectors, unit:  $\text{m}^2 \text{s}^{-2}$ ) and stream function (contour, unit:  $10^5 \text{ m}$ ) at 200 hPa regressed upon the normalized PC time series corresponding to EOF2 of winter Southeast Asian SAT variations

weather and climate anomalies over many parts of the northern Hemisphere, especially Eurasia and North America (e.g., Inoue et al. 2012; Wu et al. 2011, 2016; Chen et al. 2014b; Sun et al. 2016; Chen and Wu 2018). To confirm the possible role of the Arctic SIC in the atmospheric circulation anomalies, we display winter Arctic sea ice concentration anomalies obtained by regression upon the PC2 of winter Southeast Asian SAT variation in Fig. 14a. It is found that large negative anomalies of SIC are found around the Barents-Kara sea. Then, we define a SIC index as the region averaged SIC anomalies over  $70^\circ\text{--}84^\circ\text{N}$  and  $55^\circ\text{--}80^\circ\text{E}$ . The domain used for the definition of the above SIC index is selected based on the significant negative SIC anomaly over the Arctic in Fig. 14a. It is noted that results are generally similar for the reasonable changes of the selected domains employed to define the SIC index (not shown).

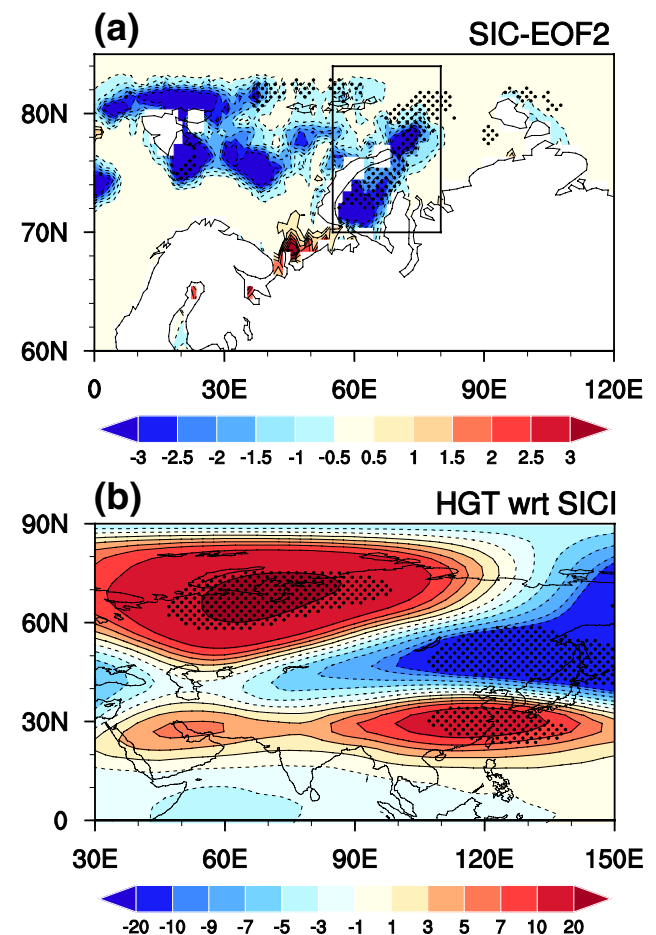


**Fig. 14 a** Anomalies of winter Arctic sea ice concentration (SIC) (unit: %) regressed upon the normalized PC time series corresponding to EOF2 of winter Southeast Asian SAT variations. **b** 200 hPa geopotential height anomalies (unit: gpm) regressed upon the SIC index. SIC index is defined as area-averaged SIC anomalies over the black box region in **(a)**. Stippling in **a**, **b** denotes anomalies that are significantly different from zero at the 95% confidence level

Figure 14b presents 200 hPa geopotential height anomalies regressed upon the defined SIC index. It shows that an apparent atmospheric wave train is observed extending from Eurasian Arctic southeastward to Southeast Asia (Fig. 14b), which is similar to the atmospheric wave train pattern originated from Arctic in Fig. 13. This implies that change in the SIC over the Arctic SIC around the Kara sea may contribute partly to the formation of the atmospheric circulation anomalies over the Southeast Asia via triggering a Rossby wave train. Detailed physical process for the influence of Arctic SIC on the Southeast Asian atmospheric circulation changes is beyond the scope of this study, and remains to be explored. In addition, from Table 1, it is noted that the EOF2 has a close connection with the Siberian high index, with the correlation coefficient being 0.55, significant at the 95% confidence level. The significant connection between the Siberian High and the EOF2 may be partly attributed to the impact of the Arctic SIC. As demonstrated by previous studies, change in the Arctic SIC can exert pronounced impacts on the East Asian winter SAT anomalies via modulating the Siberian High (Wu et al. 2011). It is noted that several studies have demonstrated a significant delayed impact of the Arctic sea ice change on the following East Asian climate (e.g., Sun et al. 2016; Zuo et al. 2016b; Chen and Wu 2018). By contrast, our present study shows that Arctic sea ice change over the Arctic Kara Sea during boreal winter has an impact on the simultaneous winter SAT anomalies over the southeast Asia. Differences in the response times of East Asian climate anomalies to the Arctic sea ice change may be partly attributed to the different analyzed regions, and due to the different physical processes induced by the Arctic sea ice. For example, several studies showed that Arctic sea ice change impacts the Eurasian climate via the stratospheric process (e.g., Kim et al. 2014; King et al. 2016; Chen and Wu 2018). By contrast, the present study indicated that winter Arctic Kara sea ice change could exert impact on the southeast Asian winter SAT anomalies via triggering a Rossby wave train. Besides the above mentioned factors, other factors may also be important in contributing to the differences which remain to be explored.

**Table 1** Correlation coefficients of the winter Siberian high (SH) index, Arctic Oscillation (AO) index, Niño3 index, Niño4 index, and Niño3.4 index with the PC1 and PC2 time series of southeast Asian SAT interannual anomalies

	SHI	AOI	Niño3	Niño4	Niño3.4
PC1	0.50***	-0.42**	-0.26	-0.37*	-0.30**
PC2	0.55***	0.23	-0.03	-0.08	-0.05

Definitions of the SH index (SHI), AO index (AOI), Niño3, Niño4, and Niño3.4 indices are provided in the text

“\*”, “\*\*”, “\*\*\*” Correlation coefficients significant at the 90% 95%, and 99% confidence level based on the two-tailed Student’s t test

### 4.3 SST changes related to EOF1 and EOF2

Atmospheric circulation anomalies related to EOF1 and EOF2 of the winter Southeast Asian SAT variation may be related to the SST changes. Winter SST and precipitation anomalies regressed upon the normalized PC time series corresponding to EOF1 and EOF2 of winter Southeast Asian SAT variations are presented in Fig. 15. Results are very similar when using the SST data from the ERSSTv3b and HadISST (Figures S1 and S2 in the supporting materials). For the EOF1, significant SST cooling anomalies are observed over the tropical central-eastern Pacific, Indian Ocean, and South China Sea, accompanied with SST warming over the subtropical western North Pacific and mid-latitudes North Pacific (Fig. 14a). This SST anomaly pattern bears a close resemblance to that related to a central Pacific type La Niña event (Wang et al. 2000; Alexander et al. 2002; Huang et al. 2004; Zhang et al. 2015; Song et al. 2017). The correlation coefficient between the PC1 time series of the southeast Asian SAT variation with the Niño3.4 (Niño4) SST indices reaches  $-0.3$  ( $-0.36$ ), significant at the 90% (95%) confidence level. By contrast, correlation of the PC1 with the Niño3 index cannot pass the 90% confidence level (Table 1). This indicates that EOF1 of the winter Southeast Asian SAT variation has a more close connection with the central Pacific than eastern Pacific type ENSO events. Marked negative precipitation anomalies are seen over the tropical central-eastern Pacific and positive precipitation anomalies appear over the subtropical western North Pacific (Fig. 15c). In particular, the positive precipitation anomalies over the western North Pacific may contribute to formation of the anomalous cyclone around the South China Sea and the Philippines via a Gill-type Rossby wave atmospheric response (Figs. 7a, 15c) (Zhang et al. 1996; Wang et al. 2000). The northerly wind anomalies to the west flank of the anomalous cyclone further partly contribute to negative SAT anomalies related to the EOF1 of winter Southeast Asian SAT variations (Figs. 2a, 7a). To further conform role of the La Niña-like SST anomalies over the tropical central-eastern Pacific in influencing the southeast Asian SAT anomalies via inducing an anomalous cyclone around the South China Sea and the Philippines, we display precipitation and 1000 hPa wind anomalies obtained by regression upon the normalized minus one Niño4 index in Fig. 16. It is noted that in response to the significant negative SST anomalies over the tropical central-eastern Pacific (not shown), significant negative precipitation anomalies are found over the tropical central Pacific (Fig. 16a). In addition, pronounced positive precipitation anomalies are seen around the tropical western North Pacific (Fig. 16a). Previous studies have demonstrated that formation of the positive precipitation anomalies around the tropical western North Pacific could be attributed to the anomalous Walker circulation induced by the negative SST

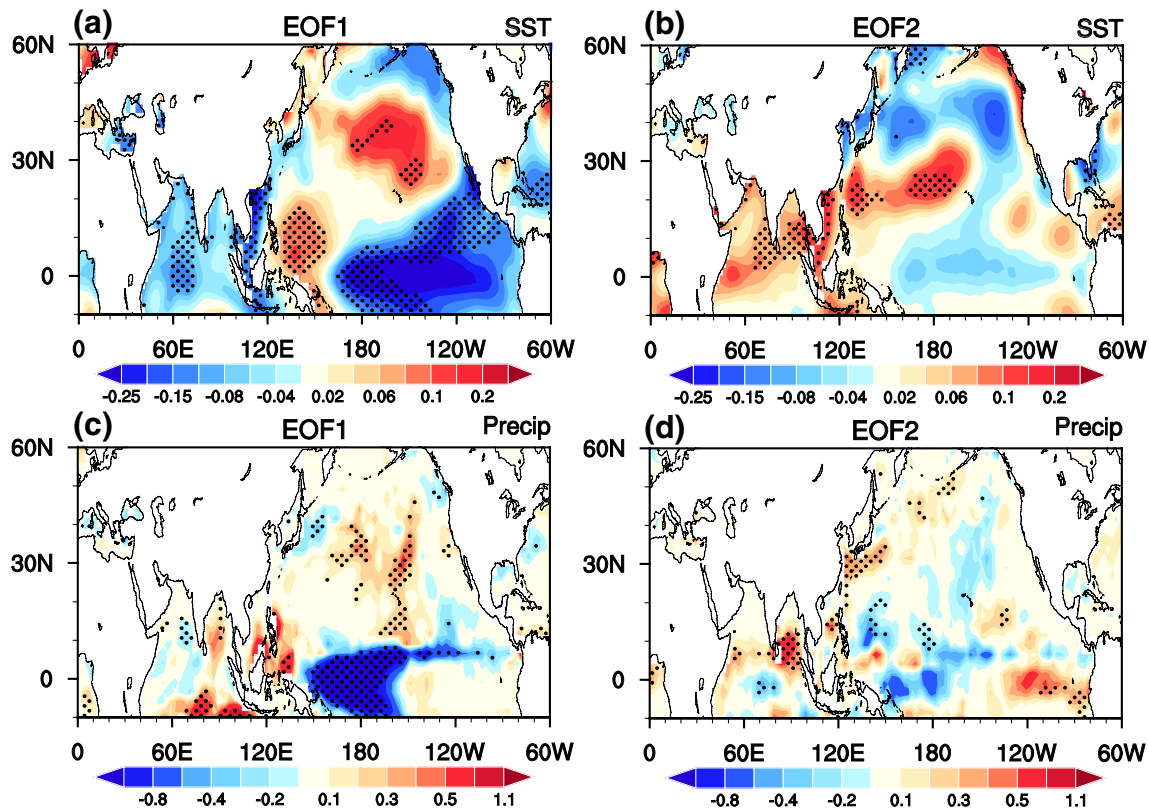


**Fig. 15** Anomalies of winter **a, b** SST (unit:  $^{\circ}\text{C}$ ) and **c, d** precipitation (unit:  $\text{mm day}^{-1}$ ) regressed upon the normalized PC time series corresponding to (left column) EOF1 and (right column) EOF2 of

winter Southeast Asian SAT variations. Stippling in **a–d** denotes anomalies that are significantly different from zero at the 95% confidence level

anomalies over the tropical central Pacific related to the La Niña event (Klein et al. 1999; Wang et al. 2000; Alexander et al. 2002). Then, the positive precipitation anomalies related to the La Niña further result in a significant cyclonic anomaly around the Philippine sea via a Gill-type atmospheric response (Fig. 16b) (Gill 1980). This result is consistent with previous findings (Wang et al. 2000; Alexander et al. 2002). The northerly wind anomalies over the southeast Asia related the anomalous cyclone further contribute to the formation of the negative SAT anomalies via carrying colder air from higher latitudes. Hence, this confirms that La Niña-like SST anomaly pattern plays a role in the formation of the SAT anomalies associated with EOF1 of winter Southeast Asian SAT.

For the EOF2, SST anomalies over the tropical Pacific are insignificant, indicating weak impact of the ENSO on the dipole SAT anomaly pattern over Southeast Asia (Figs. 2b, 15b). Pronounced SST warming anomalies are apparent over the tropical northern Indian Ocean (Fig. 15b). Correspondingly, significant positive precipitation anomalies tend to be observed over the tropical Northern Indian Ocean, indicating increase in the convection. Hence, formation of the pair of the anomalous cyclones over the tropical north and

south Indian Ocean is likely to be a Gill-type atmospheric response of the positive precipitation anomalies over the tropical Northern Indian Ocean induced by the SST warming there (Gill 1980) (Figs. 7b, 15d). The southwesterly wind anomalies related to these anomalous cyclones may be favorable for generation of positive SAT anomalies over the Indo-China Peninsula (Figs. 2b, 7b). To further confirm role of the North Indian Ocean SST anomalies for the generation of the atmospheric circulation anomalies related to the EOF2 of the southeast Asian SAT variations, we show precipitation and 1000 hPa wind anomalies obtained by regression upon the North Indian Ocean (NIO) SST index in Fig. 17. The NIO SST index is defined as the SST anomalies averaged over  $5^{\circ}$ – $15^{\circ}\text{N}$  and  $80^{\circ}$ – $100^{\circ}\text{E}$ . The region used for the definition of the NIO SST index is selected according to the significant positive SST anomaly over the Indian Ocean in Fig. 15b. From Fig. 17, it is noted that significant and large positive precipitation anomalies are found over the North Indian Ocean around  $5^{\circ}$ – $15^{\circ}\text{N}$  and  $80^{\circ}$ – $100^{\circ}\text{E}$  related to the positive SST anomalies there. Accordingly, a pair of cyclonic anomaly was observed over the tropical north and south Indian Ocean, which is likely a Gill-type atmospheric response to the atmospheric heating, leading



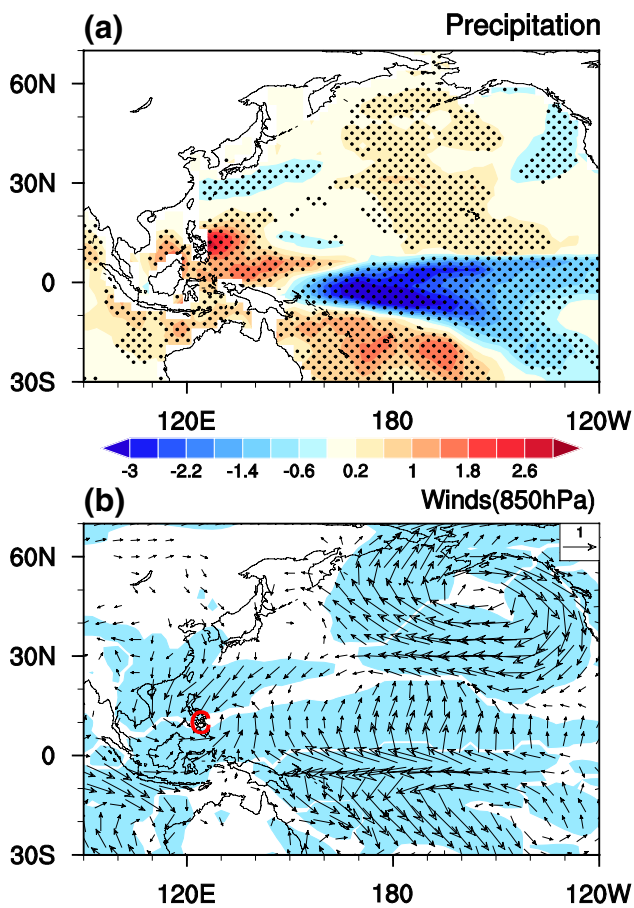


**Fig. 16** Anomalies of winter **a** precipitation (unit:  $\text{mm day}^{-1}$ ) and **b** 1000 hPa winds ( $\text{m s}^{-1}$ ) obtained by regression upon the normalized Niño4 index. Stippling in **a** denotes anomalies that are significantly different from zero at the 95% confidence level. The shading in **b** denotes regions where either component of the wind anomalies that is significantly different from zero at the 95% confidence level

to significant southwesterly wind anomalies over the tropical Indian Ocean extending eastward to the Southeast Asia (Fig. 17b). This confirms that the positive SST anomalies over the North Indian Ocean may partly contribute to the formation of the southwesterly wind anomalies around the Indo-China peninsula. Hence, above results implies that Indian Ocean SST anomalies may play a role for the SAT anomalies related to the EOF2 of the winter Southeast Asian SAT anomalies. It should be mentioned that there may exist positive interaction between the southwesterly wind anomalies and the SST warming over the tropical North Indian Ocean. In particular, the anomalous southwesterly winds induced by the SST warming would reduce the climatological northeasterly wind (Please see Figure S3 in the supporting materials). Decrease in the climatological wind speed would, in turn, maintain SST warming over the tropical North Indian Ocean via reduction of surface evaporation (Xie and Philander 1994).

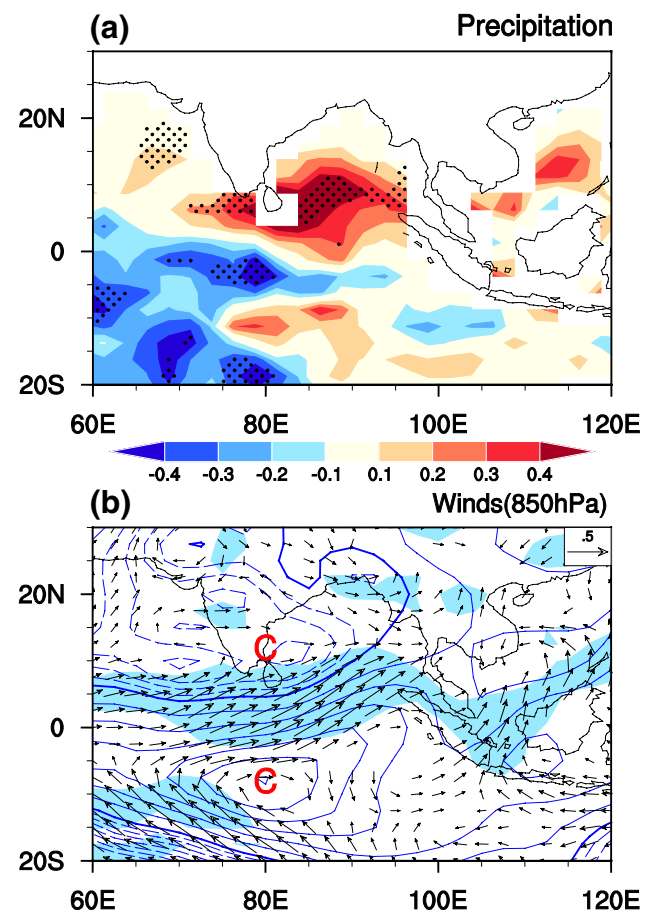


**Fig. 17** As in Fig. 16, but for **a** precipitation (unit:  $\text{mm day}^{-1}$ ) and **b** 1000 hPa winds (unit:  $\text{m s}^{-1}$ ) and stream function (contours, unit:  $10^5 \text{ m}^2 \text{ s}^{-1}$ ) anomalies obtained by regression upon the normalized Indian Ocean SST index. Definition of the Indian Ocean SST index was provided in the text. Contour interval is  $0.5 \times 10^5 \text{ m}^2 \text{ s}^{-1}$  and zero line is in bold in (b)

## 5 Summary

Using the atmospheric data from NCEP-NCAR reanalysis, ERSSTv3b SST, GPCP precipitation and sea ice concentration data from the HadISST and the SAT data provided by the University of Delaware, the leading interannual variation modes of winter Southeast Asian SAT during 1979–2014 were investigated. It is showed that SAT interannual variations are able to explain above 70% of the original SAT variations over most part of the Southeast Asian regions during 1979–2014. An EOF technique is further performed to obtain the first two dominant modes of the Southeast Asian SAT interannual variations. The first EOF mode shows same-sign SAT variations over the Southeast Asian region, with a center of action around the north part of Indo-China Peninsula and the south China. The second EOF mode displays a dipole oscillation in SAT variation between the Indo-China Peninsula and the south China. In addition, the

PC time series corresponding to the EOF1 has a significant spectral peak around 4 years. The PC2 time series shows two marked spectral peaks around 2.5 and 3.6 years, respectively.

Analysis of surface heat flux indicates that SAT anomalies over Southeast Asia related to the EOF1 cannot be explained by the surface net heat flux change. Weak surface heat flux change associated with EOF1 is attributed to the fact that increases in the surface shortwave radiation and latent heat flux are nearly cancelled by the decreases in the surface longwave radiation and sensible heat flux. For the EOF2, surface heat flux changes may partly contribute to formation of the dipole SAT variations between the Indo-China Peninsula and the south China. Decrease in the surface net heat flux over south China is mainly contributed by the surface shortwave radiation variation, while increase in the surface net heat flux over the Indo-China Peninsula is primarily attributed to change in the surface longwave radiation. Variations of surface shortwave and longwave radiations related to EOF1 and EOF2 may be related to change in the total cloud cover.

Atmospheric circulation anomalies play an important role for the SAT variations both for EOF1 and EOF2. For the EOF1, a pronounced anomalous cyclone appears over the South China Sea and around the Philippine Sea, together with significant northerly wind anomalies extending from north China southward to the Southeast Asia. These significant northerly wind anomalies bring colder air from higher latitudes and result in notable negative SAT anomalies over the Southeast Asian region. For the EOF2, a pair of significant cyclonic anomaly appears over the tropical Northern and Southern Indian Ocean, together with pronounced southerly wind or southwesterly wind anomalies over the tropical North Indian Ocean and the south part of South China Sea extending northward to the Indo-China Peninsula. These anomalous southerly or southwesterly winds carry warmer and moister air from the tropical Indian Ocean and South China Sea to the Indo-China Peninsula and contribute to significant positive SAT anomalies there. In addition, significant northeasterly wind anomalies are observed over south China, which contribute to significant negative SAT anomalies there via wind-induced temperature advection.

Further analysis shows that change in the Arctic Oscillation, Siberian High intensity, and SST anomalies over the tropical central-eastern Pacific may have a contribution to the formation of the atmospheric circulations over Southeast Asia related to the EOF1. In particular, the significant La Niña-like SST cooling over the tropical central eastern Pacific may contribute to formation of the anomalous cyclone over the South China Sea and the Philippine via Rossby wave type atmospheric response (Wang et al. 2000). Then, the northerly wind anomalies to the west side of the anomalous cycle contribute to negative SAT anomalies over the Southeast Asia. In addition, increase in the intensity

of the Siberian High may also result in northerly wind anomalies over Southeast Asia via intrusion of the Asian cold surge. Positive winter AO also partly contributes to negative SAT anomalies over southeast Asia via inducing anomalous northerly winds. The process for the impact of the winter AO on the southeast Asian atmospheric circulation and related SAT anomalies remains to be explored. For the EOF2, at the lower troposphere, two anomalous anticyclones appear over the tropical northern and southern Indian Ocean, respectively, together with significant southwesterly wind anomalies over tropical Indian Ocean extending northeastward to Indo-China Peninsula, which explain positive SAT anomalies there via wind-induced temperature advection. Generation of the anomalous cyclones over the tropical Indian Ocean may be a Rossby wave atmospheric response to the positive SST and associated enhancement of the convection over the tropical Northern Indian Ocean. In addition, the cross-equatorial flow over the South China Sea may also contribute to the southerly wind anomalies over the Indo-China Peninsula. Process for the occurrence of the cross-equatorial flow over the South China Sea is unclear and remains to be explored. At the upper troposphere, the atmospheric circulation anomalies display two clear wave trains. In particular, one wave train originates from the Mediterranean Sea propagating southeastward to North Africa and then eastward to Southeast Asia. This wave train may be excited by the upper-level convergence anomalies as identified by previous study (Watanabe 2004; Hu et al. 2017). Another wave train propagates from the Arctic Kara Sea southeastward to Southeast Asia, which may be related to the Arctic SIC variation over the Kara Sea. The physical process for the influence of the Arctic Sea ice change over the Kara Sea on the formation of the atmospheric wave train would be further pursued in the future.

**Acknowledgements** We thank two anonymous reviewers for their constructive suggestions and comments, which helped to improve the paper. This study is supported by the National Natural Science Foundation of China Grants (41661144016, 41605050, and 41530425), the Young Elite Scientists Sponsorship Program by the China Association for Science and Technology (2016QNRC001), and the China Postdoctoral Science Foundation (2017T100102 and 2015M581151). The NCEP-NCAR reanalysis data were derived from <ftp://ftp.cdc.noaa.gov/Datasets/>. The ERSSTv5 and ERSSTv3 SST data are provided by the NOAA/OAR/ESRL PSD, Boulder, Colorado, USA, from their Web site at <https://www.esrl.noaa.gov/psd/>. The GPCP precipitation data were obtained from <http://www.esrl.noaa.gov/psd/>. The University of Delaware SAT data were obtained from <https://www.esrl.noaa.gov/psd/>. The HadISST SST and sea ice concentration data were derived from <http://www.metoffice.gov.uk/hadobs/hadisst/data/>.

## References

Adler RF, Huffman GJ, Chang A, Ferraro R, Xie P, Janowiak J, Rudolf B, Schneider U, Curtis S, Bolvin D, Gruber A, Susskind

- J, Arkin P, Nelkin E (2003) The version 2 global precipitation climatology project (GPCP) monthly precipitation analysis (1979-present). *J Hydrometeorol* 4:1147–1167
- Alexander MA, Bladé I, Newman M, Lanzante JR, Lau N-C, Scott JD (2002) The atmospheric bridge: the influence of ENSO teleconnections on air–sea interaction over the global oceans. *J Clim* 15(16):2205–2231
- Bao Q, Yang J, Liu YM, Wu GX, Wang B (2010) Roles of anomalous Tibetan Plateau warming on the severe 2008 winter storm in central–southern China. *Mon Weather Rev* 138:2375–2384
- Beniston M (2004) The 2003 heat wave in Europe: a shape of things to come? An analysis based on Swiss climatological data and model simulations. *Geophys Res Lett* 31:L02202. <https://doi.org/10.1029/2003GL018857>
- Caloiero T (2017) Trend of monthly temperature and daily extreme temperature during 1951–2012 in New Zealand. *Theor Appl Climatol* 129:111–127
- Chen S, Wu R (2017) Interdecadal changes in the relationship between interannual variations of spring North Atlantic SST and Eurasian surface air temperature. *J Clim* 30:3771–3787. <https://doi.org/10.1175/JCLI-D-16-0477.1>
- Chen S, Wu R (2018) Impacts of early autumn Arctic sea ice concentration on subsequent spring Eurasian surface air temperature variations. *Clim Dyn*. <https://doi.org/10.1007/s00382-017-4026-x>
- Chen W, Graf HF, Huang RH (2000) The interannual variability of East Asian winter monsoon and its relation to the summer monsoon. *Adv Atmos Sci* 17(1):48–60
- Chen S, Yu B, Chen W (2014a) An analysis on the physical process of the influence of AO on ENSO. *Clim Dyn* 42:973–989
- Chen Z, Wu R, Chen W (2014b) Impacts of autumn Arctic sea ice concentration changes on the East Asian winter monsoon variability. *J Clim* 27:5433–5450. <https://doi.org/10.1175/JCLI-D-13-00731.1>
- Chen S, Wu R, Chen W, Yu B (2015) Influence of the November Arctic Oscillation on the subsequent tropical Pacific sea surface temperature. *Int J Climatol* 35:4307–4317. <https://doi.org/10.1002/joc.4288>
- Chen S, Wu R, Liu Y (2016a) Dominant modes of interannual variability in Eurasian surface air temperature during boreal spring. *J Clim* 29:1109–1125. <https://doi.org/10.1175/JCLI-D-15-0524.1>
- Chen W, Hong X, Lu R, Jin A, Jin S, Nam J, Shin J, Goo T, Kim B (2016b) Variation in summer surface air temperature over northeast Asia and its associated circulation anomalies. *Adv Atmos Sci* 33:1–9. <https://doi.org/10.1007/s00376-015-5056-0>
- Cheung HN, Zhou W, Mok HY, Wu MC (2012) Relationship between Ural-Siberian blocking and East Asian winter monsoon in relation to Arctic oscillation and El Niño/Southern oscillation. *J Clim* 25:4242–4257
- Choprateep S, McNeil N (2016) Surface air temperature changes from 1909 to 2008 in Southeast Asia assessed by factor analysis. *Theor Appl Climatol* 123:361–368
- Cinco T, de Guzman R, Hilario F, Wilson D (2014) Long-term trends and extremes in observed daily precipitation and near surface air temperature in the Philippines for the period 1951–2010. *Atmos Res* 145:12–26. <https://doi.org/10.1016/j.atmosres.2014.03.025>
- D'Arrigo R, Wilson R, Li J (2006) Increased Eurasian-tropical temperature amplitude difference in recent centuries: implications for the Asian monsoon. *Geophys Res Lett* 33:L22706. <https://doi.org/10.1029/2006GL027507>
- Ding Y (1987) *Monsoons over China*. Springer, New York, p 419
- Duchon C (1979) Lanczos filtering in one and two dimensions. *J Appl Meteorol* 18:1016–1022
- Feudale L, Shukla J (2010) Influence of sea surface temperature on the European heat wave of 2003 summer. Part I: an observational study. *Clim Dyn* 36:1691–1703. <https://doi.org/10.1007/s00382-010-0788-0>
- Gill AE (1980) Some simple solutions for heat-induced tropical circulation. *Q J Roy Meteorol Soc* 106:447–462
- Gong D, Wang S, Zhu J (2001) East Asian winter monsoon and Arctic oscillation. *Geophys Res Lett* 28:2073–2076
- Guan Y, Zhang X, Zheng F, Wang B (2015) Trends and variability of daily temperature extremes during 1960–2012 in the Yangtze River Basin, China. *Glob Planet Chang* 124:79–94
- He S, Wang H (2016) Linkage between the East Asian January temperature extremes and the preceding Arctic Oscillation. *Int J Climatol* 36:1026–1032
- Henderson-Sellers A (1996) Soil moisture: a critical focus for global change studies. *Global Planet Change* 13:3–9
- Holton JR (1992) *An introduction to dynamic meteorology*. Academic Press, London
- Hong CC, Li T (2009) The Extreme Cold Anomaly over Southeast Asia in February 2008: Roles of ISO and ENSO. *J Clim* 22:3786–3801. <https://doi.org/10.1175/2009JCLI2864.1>
- Hu K, Huang G, Wu R, Wang L (2017) Structure and dynamics of a wave train along the wintertime Asian jet and its impact on East Asian climate. *Clim Dyn*. <https://doi.org/10.1007/s00382-017-3674-1>
- Huang J (2004) *The methods of statistical analysis and prediction in meteorology*. China Meteorological Press, Beijing (in Chinese)
- Huang R, Sun F (1992) Impacts of the tropical western Pacific on the East Asia summer monsoon. *J Meteorol Soc Japan* 70:243–256
- Huang R, Chen W, Yang B, Zhang R (2004) Recent advances in studies of the interaction between the East Asian winter and summer monsoons and ENSO cycle. *Adv Atmos Sci* 21:407–424. <https://doi.org/10.1007/BF02915568>
- Huang WY, Wang B, Wright JS, Chen RY (2016) On the non-stationary relationship between the Siberian High and Arctic Oscillation. *Plos One* 11(6):e0158122. <https://doi.org/10.1371/journal.pone.0158122>
- Huang B, Thorne P, Banzon V, Boyer T, Chepurin G, Lawrimore J, Menne M, Smith T, Vose R, Zhang H (2017) Extended reconstructed sea surface temperature, version 5 (ERSSTv5): upgrades, validations, and intercomparisons. *J Clim* 30:8179–8205
- Inoue J, Hori ME, Takaya K (2012) The role of Barents Sea ice in the wintertime cyclone track and emergence of a warm-Arctic cold-Siberian anomaly. *J Clim* 25:2561–2568. <https://doi.org/10.1175/JCLI-D-11-00449.1>
- IPCC (2013) *Summary for policymakers. Fifth Assessment Report of the Intergovernmental Panel on Climate Change*. Cambridge University Press, Cambridge
- Jeong J, Ho C (2005) Changes in occurrence of cold surges over East Asia in association with Arctic Oscillation. *Geophys Res Lett* 32:L14704. <https://doi.org/10.1029/2005GL023024>
- Kalnay E, Kanamitsu M, Kistler R, Collins W, Deaven D, Gandin L, Iredell M, Saha S, White G, Woollen J (1996) The NCEP/NCAR 40-year reanalysis project. *Bull Am Meteorol Soc* 77:437–471
- Keellings D, Waylen P (2012) The stochastic properties of high daily maximum temperatures applying crossing theory to modeling high-temperature event variables. *Theor Appl Climatol* 108:579–590
- Kim BM, Son SW, Min SK, Jeong JH, Kim SJ, Zhang Z, Shim T, Yoon JH (2014) Weakening of the stratospheric polar vortex by Arctic sea-ice loss. *Nat Commun* 5:4646
- King MP, Hell M, Keenlyside N (2016) Investigation of the atmospheric mechanisms related to the autumn sea ice and winter circulation link in the Northern Hemisphere. *Clim Dyn* 46:1185–1195
- Klein SA, Soden BJ, Lau NC (1999) Remote sea surface temperature variations during ENSO: Evidence for a tropical atmospheric bridge. *J Clim* 12:917–932
- Kunkel KE, Roger AP, Stanley AC (1999) Temporal fluctuations in weather and climate extremes that cause economic and human health impacts: a review. *Bull Am Meteorol Soc* 80:1077–1098

- Labat D, Godd ris Y, Probst JL, Guyot JL (2004) Evidence for global runoff increase related to climate warming. *Adv Water Resour* 27:631–642
- Liu X, Yanai M (2001) Relationship between the Indian monsoon rainfall and the tropospheric temperature over the Eurasian continent. *Q J Roy Meteorol Soc* 127:909–937. <https://doi.org/10.1002/qj.49712757311>
- Matsuura K, Willmott CJ (2009) Terrestrial air temperature: 1900–2008 gridded monthly time series (version 4.01), University of Delaware Dept. of Geography Center. [http://www.esrl.noaa.gov/psd/data/gridded/data.UDel\\_AirT\\_Precip.html](http://www.esrl.noaa.gov/psd/data/gridded/data.UDel_AirT_Precip.html). Accessed 6 Aug 2015
- Miyazaki C, Yasunari T (2008) Dominant interannual and decadal variability of winter surface air temperature over Asia and the surrounding oceans. *J Clim* 21:1371–1386
- Nguyen D, Renwick J, McGregor J (2014) Variations of surface temperature and rainfall in Vietnam from 1971 to 2010. *Int J Climatol* 34:249–264
- Nirmal G (2016) Heatwave in Asia: coffee crops die in Vietnam, Thai rice yield shrinks. <http://www.asianews.network/content/heatwave-asia-coffee-crops-dievietnam-thai-rice-yield-shrinks-15252>
- Nitta T (1987) Convective activities in the tropical western Pacific and their impact on the Northern Hemisphere summer circulation. *J Meteorol Soc Japan* 65:373–390
- North GR, Moeng FJ, Bell TL, Cahalan RF (1982a) The latitude dependence of the variance of zonally averaged quantities. *Mon Weather Rev* 110:319–326
- North GR, Bell TL, Cahalan RF, Moeng FJ (1982b) Sampling errors in the estimation of empirical orthogonal functions. *Mon Weather Rev* 110:699–706
- Rayner NA, Parker DE, Horton EB, Folland CK, Alexander LV, Rowell DP, Kent EC, Kaplan A (2003) Global analyses of sea surface temperature, sea ice, and night marine air temperature since the late nineteenth century. *J Geophys Res* 108:4407
- Smith TM, Reynolds RW, Peterson TC, Lawrimore J (2008) Improvements to NOAA’s historical merged land-ocean surface temperature analysis (1880–2006). *J Clim* 21:2283–2296
- Song L, Chen S, Chen W, Chen X (2017) Distinct impacts of two types of La Ni a events on Australian summer rainfall. *Int J Climatol* 37:2532–2544. <https://doi.org/10.1002/joc.4863>
- Stott PA, Stone DA, Allen MR (2004) Human contribution to the European heatwave of 2003. *Nature* 432:610–614. <https://doi.org/10.1038/nature03089>
- Sun Y, Zhang X, Zwiers F, Song L, Wan H, Hu T, Yin H, Ren G (2014) Rapid increase in the risk of extreme summer heat in Eastern China. *Nat Clim Change* 4:1082–1085
- Sun C, Yang S, Li WJ, Zhang R, Wu R R (2016) Interannual variations of the dominant modes of East Asian winter monsoon and possible links to Arctic sea ice. *Clim Dyn* 47:481–491
- Takaya K, Nakamura H (1997) A formulation of a wave-activity flux for stationary Rossby waves on a zonally varying basic flow. *Geophys Res Lett* 24:2985–2988
- Takaya K, Nakamura H (2001) A formulation of a phase-independent wave-activity flux for stationary and migratory quasigeostrophic eddies on a zonally varying basic flow. *J Atmos Sci* 58:608–627
- Thirumalai K, Dinezio PN, Okumura Y, Deser C (2017) Extreme temperatures in Southeast Asia caused by El Ni o and worsened by global warming. *Nat Commun* 8:15531. <https://doi.org/10.1038/ncomms15531>
- Thompson DW, Wallace JM (1998) The Arctic Oscillation signature in the wintertime geopotential height and temperature fields. *Geophys Res Lett* 25:1297–1300. <https://doi.org/10.1029/98GL00950>
- Thompson DWJ, Wallace JM (2000) Annular Modes in the extratropical circulation. Part I: month-to-month variability. *J Clim* 13:1000–1016
- Wang B, Wu R, Fu X (2000) Pacific–East Asia teleconnection: how does ENSO affect East Asian climate? *J Clim* 13:1517–1536
- Watanabe M (2004) Asian jet waveguide and a downstream extension of the North Atlantic oscillation. *J Clim* 17:4674–4691. <https://doi.org/10.1175/JCLI-3228.1>
- Wu B, Wang J (2002) Winter Arctic Oscillation, Siberian high and East Asian winter monsoon. *Geophys Res Lett* 29:1897. <https://doi.org/10.1029/2002GL015373>
- Wu BY, Su JZ, Zhang RH (2011) Effects of autumn–winter Arctic sea ice on winter Siberian High. *Chin Sci Bull* 56:3220–3228. <https://doi.org/10.1007/s11434-011-4696-4>
- Wu ZW, Li XX, Li YJ, Li Y (2016) Potential influence of Arctic sea ice to the interannual variations of East Asian spring precipitation. *J Clim* 29:2797–2813
- Xia J, Tu K, Yan Z, Qi Y (2016) The super-heat wave in eastern China during July–August 2013: a perspective of climate change. *Int J Climatol* 36:1291–1298
- Xie SP, Philander SGH (1994) A coupled ocean–atmosphere model of relevance to the ITCZ in the eastern Pacific. *Tellus Ser A Dyn Meteorol Oceanol* 46:340–350
- Yao PZ (1995) The climate features of summer low temperature cold damage in northeast China during recent 40 years (in Chinese). *J Catastrophol* 10:51–56
- Ye L, Yang G, Van Ranst E, Tang H (2013) Time-series modeling and prediction of global monthly absolute temperature for environmental decision making. *Adv Atmos Sci* 30:382–396
- Zhang R, Sumi A, Kimoto M (1996) Impact of El Ni o on the East Asian monsoon. *J Meteorol Soc Japan* 74:49–62
- Zhang Y, Sperber KR, Boyle JS (1997) Climatology and interannual variation of East Asian winter monsoon: Result from the 1979–95 NCEP/NCAR reanalysis. *Mon Weather Rev* 125:2605–2619
- Zhang W, Wang L, Xiang B, Li Q, He J (2015) Impacts of two types of La Ni a on the NAO during boreal winter. *Clim Dyn* 44:1351–1366
- Zuo Q, Gao S, Sun X (2016a) Effects of the upstream temperature anomaly on freezing rain and snowstorms over southern China in early 2008. *J Meteorol Res* 30:694–705
- Zuo J, Ren HL, Wu BY, Li WJ (2016b) Predictability of winter temperature in China from previous autumn Arctic sea ice. *Clim Dyn* 47:2331–2343
- Zveryaev II, Aleksandrova MP (2004) Differences in rainfall variability in the South and Southeast Asian summer monsoons. *Int J Climatol* 24:1091–1107
- Zveryaev II, Gulev SK (2009) Seasonality in secular changes and interannual variability of European air temperature during the twentieth century. *J Geophys Res* 114:D02110. <https://doi.org/10.1029/2008JD010624>